ENGR 6201 Fluid Mechanics

Numerical Analysis of Characteristics for Unsteady Incompressible Viscous Flow Using the Navier-Stokes Equations

Instructor:

Dr. Alejandro Allievi

Submitted by Group 9:

Rahul Chug (Student ID: 40075138)

Mohammad Amin Amani Farani (Student ID: 40029159)

Lina Liu (Student ID: 40074560)

Yomna Gobran (Student ID: 40075118)

December, 2018

ABSTRACT

Navier-Stokes Equations describe the characteristics of the viscous fluid flow which can be identified by discretizing and solving the N-S equations using computational fluid dynamics [1]. This paper will analyze the performance of two different two-dimensional viscous flow cases by solving the unsteady incompressible N-S equations in ANSYS Fluent. The first case is lid driven square cavity considered at different Reynolds numbers. The streamlines and velocity component along the mid vertical line & horizontal line will be presented. The second case is flow around a circular cylinder simulated at Re=100. The streamlines and drag and lift force coefficients will be assessed. Finally, all the numerical results will be compared with the results published by Allievi and Bermejo [2].

Keywords: computational fluid dynamics; incompressible viscous flow

Contents

Nomenclature

Symbols	Unit	Description
p	[pa]	pressure
Re	[-]	Reynolds number
v	[m/s]	velocity
x,y,z	[-]	Cartesian coordinate axes
μ	[pa·s]	dynamic viscosity
D	[m]	diameter

Subscripts

in	inlet
out	outlet

Abbreviations

BC	boundary condition
RMS	root mean square

List of Figures

List of Tables

CHAPTER 1: INTRODUCTION

1.1 Background

‘The flow of a river never ceases to go past, nevertheless it is not the same water as before. Bubbles floating along on the stagnant water now vanish and then develop but have never remained [3]. Fluid Dynamics is such a discipline that studies the effects of force on fluid motion from a macroscopic point of view, involving fluid flow, heat transfer, and other related physical phenomena [4].

Computational fluid dynamics (CFD) is a branch of fluid mechanics that uses different numerical analysis methods to solve and analyze flow phenomenon. The emergence of computational fluid dynamics has promoted the development of fluid machinery research which was originally developed from the pioneering accomplishments of enthusiasts such as Richardson (1910) and Courant, Friedrichs, and Lewy (1928). With the rapid development of computer technology, CFD technology has developed rapidly and has gradually become an important means of product development along with experimental fluid mechanics.

The Finite Volume Method (FVM) is one of the widely used numerical techniques in solving the partial differential equations in the conservation laws of fluid dynamics. This method transforms differential volume into discrete algebraic equation on finite volume. Then, the algebraic equations are solved to calculate the dependent variables of each element to represent the physical process. ANSYS Fluent is a commercial CFD code based on finite volume method, which contains many turbulence models and can simulate the steady or unsteady state of viscous or non-viscous fluids.

1.2 Project Description

The objective of this study is to use a finite volume method in ANSYS Fluent to estimate the values of the fluid flow characteristics for the following two cases:

Case A. Lid-driven square cavity flow: We are solving for an incompressible unsteady, viscous flow, from *Re*=100 to 10,000. The cavity dimensions in all directions are equal to unity. The lid horizontal velocity is assumed to be unity, constant afterwards. Calculations will be carried out with time step = 0.1 for a total time of 150 seconds. Different meshes will be studied till we match the results well. Lastly, the streamline contours and velocity profiles at the mid-lines of the cavity will be plotted and the number of iterations required for different *Re* numbers will be presented.

Case B. Flow around a circular cylinder: We will simulate two-dimensional incompressible unsteady, viscous flow around a circular cylinder at *Re*=100. The circular cylinder is positioned inside a straight channel with rigid boundaries. The boundary conditions are uniform flow at the inlet, zero velocity at the rigid boundaries and at the open boundary. Simulations will be carried out at a time step of 0.1 for 3000 time steps. At the end, the streamline contours will be plotted at different time instances, as well as the lift and drag coefficients.

1.3 Paper Organization

This report is organized in 5 chapters. Chapter 1 presents an introduction to the project. Chapter 2 provides a literature review on the state-of-the-art in the methodology, modeling and CFD tool. Chapter 3 presents the problem specification to achieve the proposed objectives while chapter 4 presents the results and discussions. Finally, Chapter 5 gives the conclusions from the work done so far.

CHAPTER 2: LITERATURE REVIEW

This chapter provides a literature review of previous work related to lid-driven square cavity flow and flow around a circular cylinder.

2.1 Lid-Driven Square Cavity Flow

Lid-driven square cavity flow is a classical topic of great interest due to its wide range of applications such as electronic device cooling, high-performance building insulations, drying technologies, etc. The review of the literature on lid driven cavity flow indicates two categories of previous work: experimental and computational.

2.1.1 Experimental Analysis of Lid-Driven Square Cavity Flow

Experimental studies focusing on fluid flow behavior in the cavity have been carried out for several years. With the development of the Laser Doppler Anemometer and particle image velocimetry techniques, it became possible to visualize the transient behavior of the flow [5].

In 1984, Koseff and Street [6,7] conducted an investigation in the lid-driven cavity with depth-to-width ratio of 1:1 and the span-to-width ratio of 3:1, 2:1 and 1:1. They used the thymol blue technique and by rheoscopic liquid illuminated by laser-light sheets to carry out flow visualization (see Figure 2-1). They found that the corner vortices presented at the end walls were the main factors affecting the size of the vortices, as shown in Figure 2-2. In addition, when the Reynolds number was greater than 3000, the size of the downstream secondary vortices decreased with the increase of the Reynolds number.

The lid-driven flow involves various types of instabilities at low Reynolds numbers. It has been experimentally observed that the local Taylor instability occurs near the downstream lip of the lid. In 2002, Migeon [8] used particle streak technique to study the development of vortices inside a rectangular cavity of aspect ratio 1:1:2 and Reynolds numbers 1,000, 2,000, and 3,000 where the vertical walls acted as moving lids (in Figure 2-3).

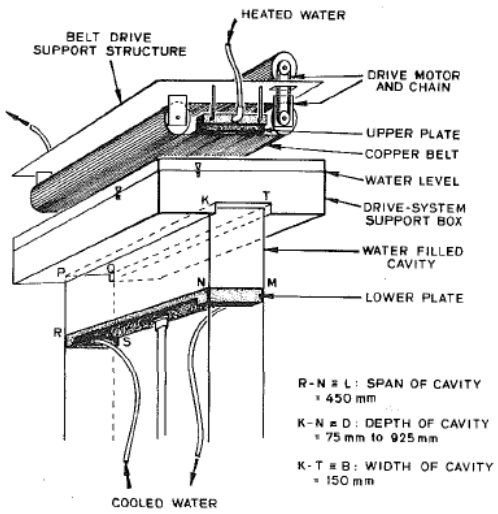

Figure 2-1 Schematic of lid-driven cavity [6]

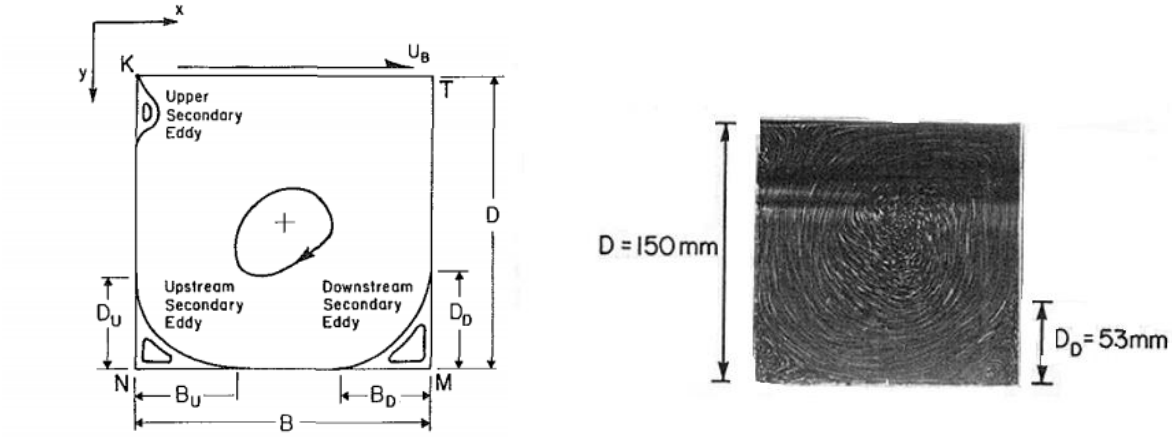

Figure 2-2 Flow in symmetry plane for Re = 3,300, spanwise-aspect-ratio = 3:1 [7]

The study provided the first visual evidence that the counter-rotating vortices were developed in four stages at Re=3,200. The first corresponded to a mixing-process reduction, the second to the formation of a structure characterized by the convergence of streamlines in span planes, the third to the in-formation of the streamlines, and the fourth to the formation of the counter-rotating structures. However, at Re=1,000 and 2,000, the instability development stopped at the second and third phase, respectively.

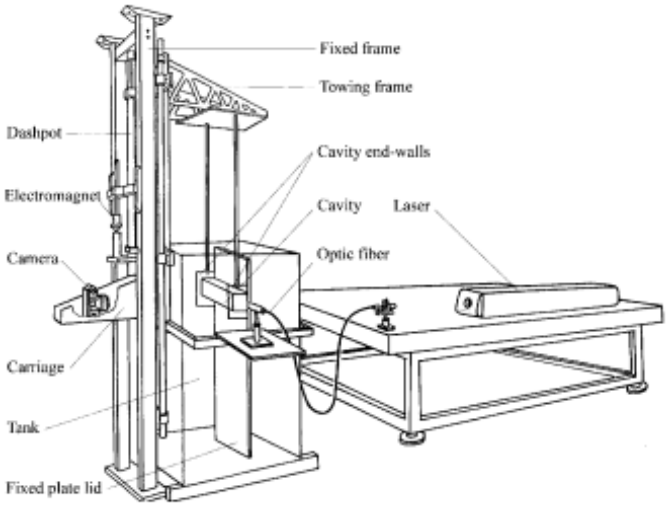

Figure 2-3 Schematic of vertical lid-driven cavity [8]

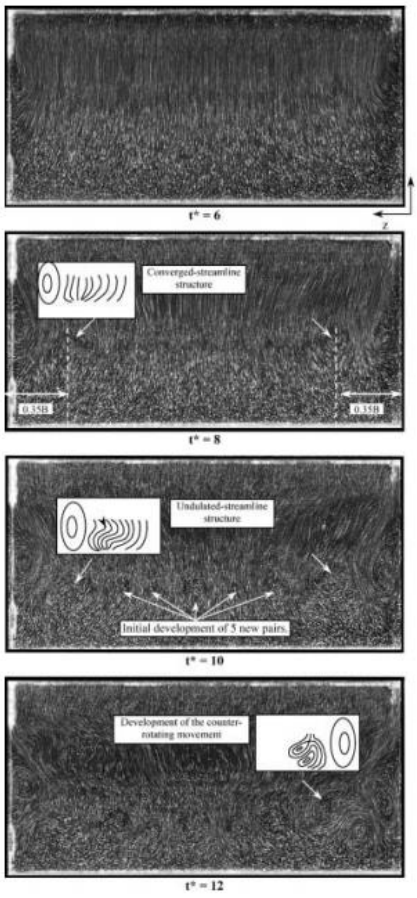

Figure 2-4 Visualizations of the mid-span section for Re=3,200 [8]

2.1.2 Numerical Method Analysis of Lid-Driven Square Cavity Flow

After the development of the CFD technology and computer processing ability, CFD simulation plays an increasingly important role in studying the flow physics. In the section, three discretization techniques will be introduced, such as the Finite Difference Method, the Finite Volume Method and the Finite Element Method. After the long-term comparisons with the experimental results, the CFD method is reliable and can predict fluid phenomena accurately.

Finite difference method [9] is the earliest method used in computer numerical simulation, and it is still widely used. This method divides the solution domain into difference grids and replaces the continuous solution domain with finite grid nodes. By using Taylor series expansion and other methods, the derivatives of the governing equations are discretized by the difference quotient of the function values on the grid nodes and then the algebraic equations with the unknown values on the grid nodes are established. This method is an approximate numerical solution that directly transforms differential problems into algebraic problems. It has intuitive mathematical concepts and simple expression. It is an early and mature Numerical method. For finite difference schemes, there are first-order schemes, second-order schemes and higher-order schemes. Considering the spatial form of difference, it can be divided into central scheme and inverse scheme. Considering the influence of time factor, the difference schemes can also be divided into explicit schemes, implicit schemes and explicit-implicit alternating schemes. At present, the common difference schemes are mainly the combination of the above-mentioned forms. Different combinations form different difference schemes. The difference method is mainly applicable to structured grids. The step size of the grids is usually determined by the actual terrain and Collan stability conditions. There are many ways to construct the difference. At present, the Taylor series expansion method is mainly used. There are three basic differential expressions: first-order forward difference, first-order backward difference, first-order central difference and second-order central difference. The first two schemes are the first-order accuracy, and the last two schemes are second-order accuracy. By combining the different difference schemes of time and space, different difference schemes can be combined. Bruneau and Saad [10] presented steady and periodic solutions for various Reynolds numbers from 1,000 to 10,000 by solving the unsteady Navier-Stokes equations on a 1024 x 1024 uniform 2-D grid. The streamline results were shown in Figure 2-5. Their numerical simulation lied on a multigrid solver with a cell-by-cell relaxation procedure. Classical Euler or Gear time schemes were coupled to a second-order approximation of the linear terms in space. Convective terms were treated explicitly and approximated by third-order schemes.

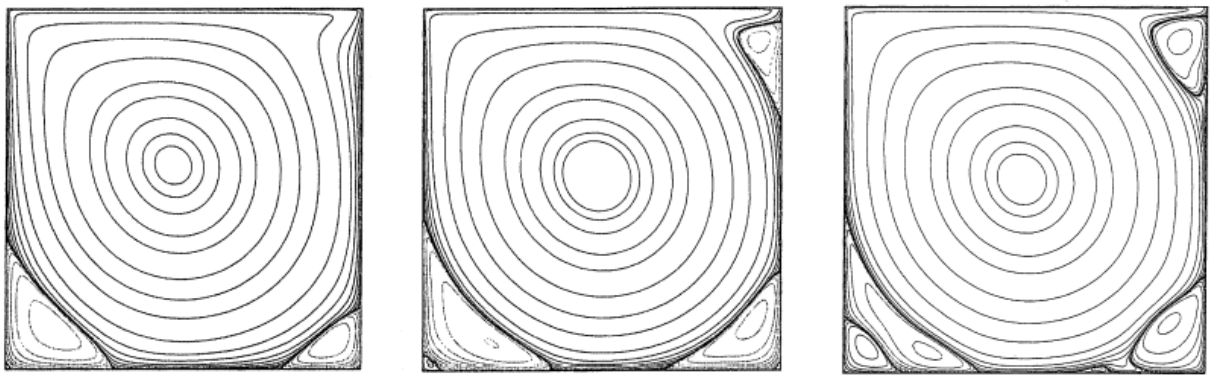

Figure 2-5 Streamlines at Re=1,000, 5,000 and 10,000 [10]

The finite volume method [11] is also called the control volume method. The theory will be introduced in Section 3.1. Wright and Gaskell [12] solved 2-D incompressible laminar flow in a lid-driven cavity using a second and fourth order spatially accurate steady solution at Reynolds number from 100 to 1,000, staggered grid arrangement and control volume formulation. They used the Block Implicit Multigrid Method [24] on a uniform mesh of 1024 x 1024. The streamline results were shown in Figure 2-6. By comparing Figure 2-5 and Figure 2-6 at Re=1,000, it was found that the streamline contours were similar.

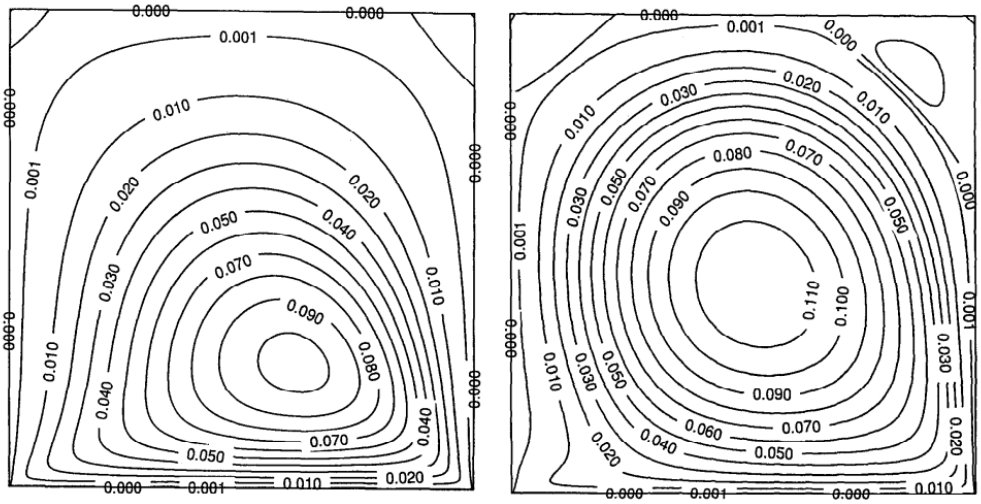

Figure 2-6 Streamlines at Re=100 and 1,000 [12]

The basic idea of the finite element method [14] is to divide the computational domain into finite non-overlapping units. Within each element, some suitable nodes are selected as interpolation points for solving functions, and the variables in the differential equation are rewritten to the node values of each

variable or its derivatives and the selected ones. With the help of the variational principle or weighted residual method, the differential equation is solved by the discrete method. Barragy and Carey [15] presented the 2-D driven cavity incompressible flow at Reynolds number from 5,000 to 16,000 by using finite element scheme fully coupled stream function vorticity formulation of the Navier-Stoke equations. They observed a significant feature that new tertiary and quaternary corner vertex features, as shown in Figure 2-7.

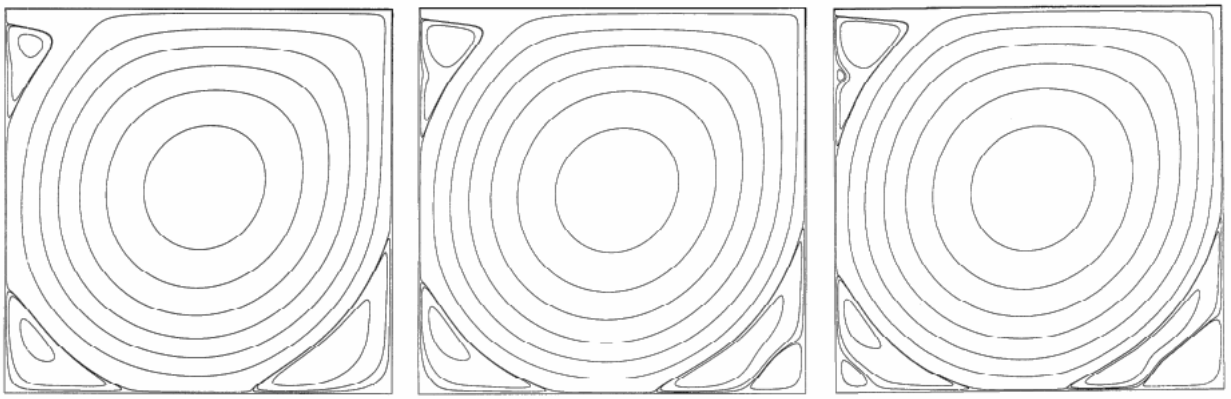

Figure 2-7 Streamlines at Re= 5,000, 10,000, and 16,000 [15]

Many authors [16-18] have solved similar problems for incompressible fluids moving with low and medium Reynolds number (upto 10,000) in the past few decades, but the study of the high Reynolds number is on rise considering its numerous applications [19].

The study of incompressible flow has been the benchmark for years with widespread applications for the researchers including the study of channel flows, cavity flows with low and high Mach number in laminar flows. In recent years, the interest was also shown towards other methods like cell based smoothed (CBS) FEM to solve the incompressible Navier- stokes equations [20].

The lid driven cavity flow problem is commonly used as a guideline for numerical methods due to its simple geometry but complex fluid dynamics behavior, and it has been carefully addressed by several investigators [21-24]. Moreover, researches have also been conducted dealing with the oscillatory movement of the lid in transient situations [25] in the lid driven cavity flow. Goodrich and Soh [26] also studied the lid driven flow in a square cavity using a time-accurate finite difference method to solve unsteady incompressible Navier–Stokes equations in the form of primitive variables.

2.2 Flow Around A Circular Cylinder

It is unlikely to find an analytical description of solutions of real flow problems. Even for academic test examples which try to mimic at least some features of real flows, like the test problem chosen in this paper, analytical solutions are not known generally. There are two ways to provide reference data for such problems. The first one consists in the measurement of quantities of interest in experiments. The second way is to perform careful numerical studies with highly accurate discretizations. The development of high-performance computers in the recent decades made this way feasible. An advantage of this approach is that in the reference data no measurement errors are present.

The Navier–Stokes equations are the fundamental equations of fluid dynamics. Many schemes for their numerical solution have been developed and probably will be developed. These schemes have to be tested at appropriate examples. ANSYS FLUENT will be used in this study.

This project presents a numerical study of a time-dependent two-dimensional flow through a channel around a cylinder. Its main objective is to provide accurate reference values for the mean drag and lift coefficient at the cylinder. In addition, the accuracy of these values obtained are compared with results from literature.

The definition of this test problem is simple such that it can be implemented easily in each code. The flow possesses features which often occur in real flow problems like the vortex shedding and separation of flow.

2.2.1 Experimental and numerical analysis of flow Around A Circular Cylinder

The study of the flow around a circular cylinder has been done a lot in the literature because Flow around cylindrical structures is of relevance for many practical applications, e.g. offshore risers, bridge piers, periscopes, chimneys, towers, masts, stays, cables, antennae and wires. Knowledge about flow-related unsteady loading on such structures is crucial for hydro- and aerodynamic design and control. In addition it is a used as a test for computational fluid models.

Allievi and Bermejo [2] presented numerical test for the incompressible viscous flow around a circular cylinder at Reynolds number = 100, with the intention of clearly demonstrating the performance of finite element modified method of characteristics (FEMMC) algorithm and with presenting a comparison with other numerical and experimental results. A relatively coarse mesh was used with 1295 nodes, for a total of 3000 iterations with a time step of 0.01. For this mesh, the number of iterations required for the scheme to converge to a tolerance of 10^{-3} in the maximum norm, were less than 20 iterations in 83% of

the entire run. The mean drag coefficient was = 1.295, while the RMS lift coefficient was ±0.162 with a Strouhal number = 0.167.

Harichandan and Roy [27] conducted an incompressible unsteady viscous two-dimensional finite volume Navier–Stokes solver is developed using ‘‘consistent flux reconstruction” technique on a collocated unstructured mesh comprising of triangular cells. In this solver, the full Navier–Stokes equations have been solved numerically in the physical plane itself without using any transformation to the computational plane. The cell face centre velocities are reconstructed explicitly by solving the momentum equations on flux reconstruction control volumes defined judiciously around the respective cell face centres. This is followed by solution of the cell centre pressure field using a discrete Poisson equation developed from the reconstructed velocities and updating the cell centre velocities by using an explicit scheme. The solver has been applied to unconfined flow past a single cylinder at Re = 100 and 200 to validate the numerical code. A triangular mesh comprising of 29,464 cells and 14,878 nodes out of which 160 nodes are on the body surface was used. The non-dimensional time step used in the calculation is 0.001. At every time level, the convergence criteria for pressure-Poisson equation is set in a manner that the residual is less than 10^{-6}. To obtain the characteristics of lift and drag coefficients, simulation was performed up to 400 non-dimensional time. For Re = 100, the mean drag coefficient was = 1.4.

Another study to investigate the flow structures around a circular cylinder uses an implicit pressure-based finite volume method for time-accurate computation of incompressible flow using second order accurate convective flux discretization schemes Rajani et al. [28]. The Reynolds number investigated were between 5 and 260 to identify when 3-D effects are not to be ignored. The grid is polar with 144 nodes stretched along the radial direction and 121 equi-spaced nodes around the circumferential direction, periodic boundary conditions are used at the end planes. Calculations were done with a time step = 0.05. The mean drag coefficient was = 1.45.

The flow past a circular cylinder at Re = 50-200 was studied because of its fundamental importance and its relevance for practical applications Qu [29]. A polar grid was used in the vicinity of the cylinder with a computational time step = 0.005. The mean drag coefficient was = 1.319, while the RMS lift coefficient was ±0.225 with a strouhal number = 0.1648.

CHAPTER 3: PROBLEM SPECIFICATION

3.1 Theory

The objective of the project is to model viscous flow in the same geometry and conditions as Allievi and Bermejo [2] by solving the Navier-Stokes equations with appropriate boundary conditions using the Ansys Fluent CFD software which uses the Finite Volume Method. The basic idea of the finite volume method is to divide the computational region into a series of non-repetitive control volumes and make each grid point surrounded by a control volume. By integrating the differential equation to be solved with each control volume, a set of discrete equations can be obtained. The unknown is the value of the dependent variable at the grid point. In order to obtain the integral of the control volume, it is necessary to assume that the distribution profile of the hypothetical value is divided into segments. From the point of view of the selection method of integral region, the finite volume method belongs to the sub-region method of weighted residuals and from the point of view of the approximation method of unknown solution, the finite volume method belongs to the discrete method of local approximation. In short, the sub-region method belongs to the basic method of finite volume generation.

3.2 Introduction to Ansys Fluent

ANSYS Fluent is a state-of-the-art computer program for modeling fluid flow, heat transfer, and chemical reactions in complex geometries. It provides complete mesh flexibility, including the ability to solve flow problems using unstructured meshes that can be generated about complex geometries with relative ease. Supported mesh types include 2-D triangular / quadrilateral, 3-D tetrahedral / hexahedral / pyramid / wedge / polyhedral, and mixed (hybrid) meshes. ANSYS Fluent also enables the user to refine or coarsen the mesh based on the flow solution. Mesh can either be read into ANSYS Fluent, or created using the “Mesh” module of Fluent. All remaining operations are performed within the “Solution” module, including setting boundary conditions, defining fluid properties, executing the solution, refining the mesh, and postprocessing and viewing the results.

The ANSYS Fluent serial solver manages file input and output, data storage, and flow field calculations using a single solver process on a single computer. ANSYS Fluent also uses a utility called cortex that manages the user interface and basic graphical functions. Its parallel solver enables users to compute a solution using multiple processes that may be executing on the same computer, or on different computers in a network. Parallel processing in ANSYS Fluent involves an interaction between ANSYS

Fluent, a host process, and a set of compute-node processes. ANSYS Fluent interacts with the host process and the collection of compute nodes using the cortex user interface utility.

The complete solution process of ANSYS Fluent is shown in Figure 3-1. In the first step, we need to conduct pre-analysis to obtain the boundary conditions and the required data for representing the real case. The “Geometry” module is used to generate the geometry model in ANSYS workbench or any other CAD software, such as AutoCAD, Solidworks, NX Nastran, CATIA, etc. Meshing quality determines the accuracy of the result. different parameters that control the solution accuracy, boundary conditions, physics involved, material characteristics, etc. are entered in the “Physics Setup” module. In the “Solution” module, the solver will calculate the equations iteratively, updating the guess after each iteration, and stopping the iterations when imbalances are below a preconfigured tolerance. And finally, the “Results” module is used for post-processing and analysis of the results.

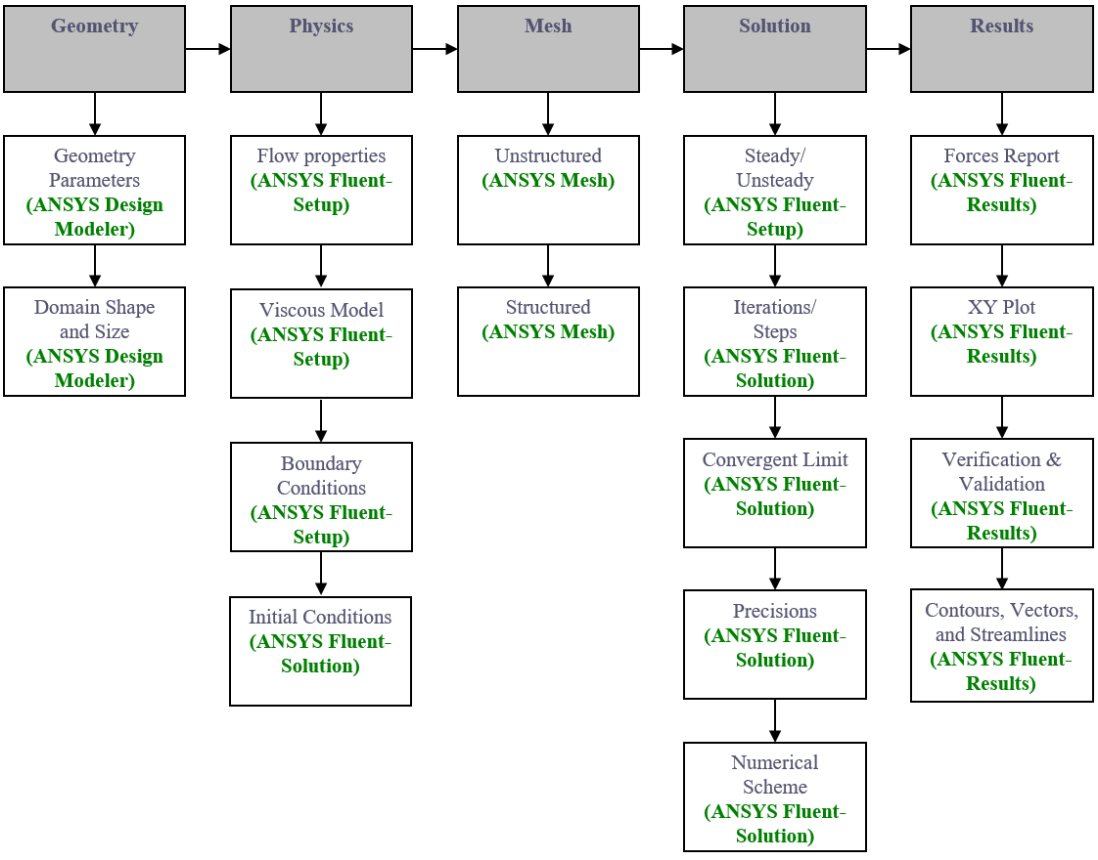

Figure 3-1 ANSYS Fluent process [30]

3.3 Equations

3.3.1 The Mass Conservation Equation

The equation for conservation of mass, or continuity equation, can be written as follows:

$$\frac{\partial \rho}{\partial t} + \nabla \cdot (\rho \vec{v}) = S_m \tag{1.1}$$

The source Sm is the mass added to the continuous phase from the dispersed second phase (for example, due to vaporization of liquid droplets) and any user-defined sources.

For 2-D axisymmetric geometries, the continuity equation is given by

$$\frac{\partial \rho}{\partial t} + \frac{\partial}{\partial x}(\rho v_x) + \frac{\partial}{\partial r}(\rho v_r) + \frac{\rho v_r}{r} = S_m \tag{1.2}$$

Where x is the axial coordinate, r is the radial coordinate, v_x is the axial velocity, and v_r is the radial velocity.

3.3.2 Momentum Conservation Equation

Conservation of momentum in an inertial (non-accelerating) reference frame is given by

$$\frac{\partial}{\partial t}(\rho \vec{v}) + \nabla \cdot (\rho \vec{v}\,\vec{v}) = -\nabla p + \nabla \cdot (\bar{\bar{\tau}}) + \rho \vec{g} + \vec{F} \tag{1.3}$$

where p is the static pressure, $\bar{\bar{\tau}}$ is the stress tensor (described below), and $\rho \vec{g}$ and $\vec{F}$ are the gravitational body force and external body forces (for example, that arise from interaction with the dispersed phase), respectively. $\vec{F}$ also contains other model-dependent source terms such as porous-media and user-defined sources.

The stress tensor $\bar{\bar{\tau}}$ is given by

$$\bar{\bar{\tau}} = \mu \left[\left(\nabla \vec{v} + \nabla \vec{v}^{\,T} \right) - \frac{2}{3} \nabla \cdot \vec{v}\, I \right] \tag{1.4}$$

where μ is the molecular viscosity, I is the unit tensor, and the second term on the right hand side is the effect of volume dilation.

For 2-D axisymmetric geometries, the axial and radial momentum conservation equations are given by

$$\frac{\partial}{\partial t}(\rho v_x)+\frac{1}{r}\frac{\partial}{\partial x}(r\rho v_x v_x)+\frac{1}{r}\frac{\partial}{\partial r}(r\rho v_r v_x)= -\frac{\partial p}{\partial x} +\frac{1}{r}\frac{\partial}{\partial x}\left[r\mu\left(2\frac{\partial v_x}{\partial x}-\frac{2}{3}(\nabla\cdot\vec{v})\right)\right] +\frac{1}{r}\frac{\partial}{\partial r}\left[r\mu\left(\frac{\partial v_x}{\partial r}+\frac{\partial v_r}{\partial x}\right)\right]+F_x \tag{1.5}$$

and

$$\frac{\partial}{\partial t}(\rho v_r)+\frac{1}{r}\frac{\partial}{\partial x}(r\rho v_x v_r)+\frac{1}{r}\frac{\partial}{\partial r}(r\rho v_r v_r)= -\frac{\partial p}{\partial r} +\frac{1}{r}\frac{\partial}{\partial x}\left[r\mu\left(\frac{\partial v_r}{\partial x}+\frac{\partial v_x}{\partial r}\right)\right] +\frac{1}{r}\frac{\partial}{\partial r}\left[r\mu\left(2\frac{\partial v_r}{\partial r}-\frac{2}{3}(\nabla\cdot\vec{v})\right)\right] -2\mu\frac{v_r}{r^2}+\frac{2}{3}\frac{\mu}{r}(\nabla\cdot\vec{v})+\rho\frac{v_z^2}{r}+F_r \tag{1.6}$$

where

$$\nabla\cdot\vec{v}=\frac{\partial v_x}{\partial x}+\frac{\partial v_r}{\partial r}+\frac{v_r}{r} \tag{1.7}$$

and v_z is the swirl velociy.

3.3.3 Physics of Swirling and Rotating Flows

In swirling flows, conservation of angular momentum (rw=constant) tends to create a free vortex flow, in which the circumferential velocity increases sharply as the radius decreases.

$$\frac{\partial p}{\partial r}=\frac{\rho w^2}{r}$$

3.4 Boundary Conditions

3.4.1 Boundary Conditions of Lid-Driven Square Cavity Flow

Left wall: U=0, V=0

Right wall: U=0, V=0

Top wall: U=1, V=0

Bottom wall: U=0, V=0

3.4.2 Boundary Conditions of Flow Around A Circular Cylinder

Inlet: U=1, V=0

Top wall: U=0, V=0

Bottom wall: U=0, V=0

Cylinder: U=0, V=0

Outlet: $-pn + \nu(\partial u/\partial n) = 0$

3.5 Numerical Methodology

3.5.1 Lid-Driven Square Cavity Flow

First the “Geometry” module in ANSYS Fluent has been used to create the 2-D geometry of the cavity with all directions set equal to unity. Figure 3-2 shows the 2-D cavity geometry. Next, using the “Mesh” module, two different meshes have been defined to match those of Allievi and Bermejo [2]. Figure 3-3 shows the coarse 30x30 mesh and the refined 62x40 mesh. The simulation parameters have been set in the “Setup” module, and shown in Table 3-1. These values have been chosen in such a way as to match the Reynold number, Residual criteria and other problem characteristics used in Allievi and Bermejo [2]. Finally the simulation has been run until convergence was achieved.

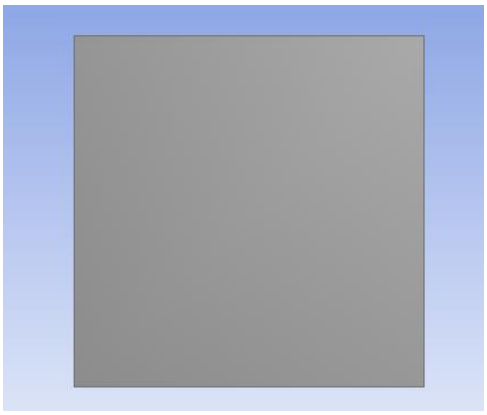

Figure 3-2 The 2-D cavity geometry, 1m x 1m

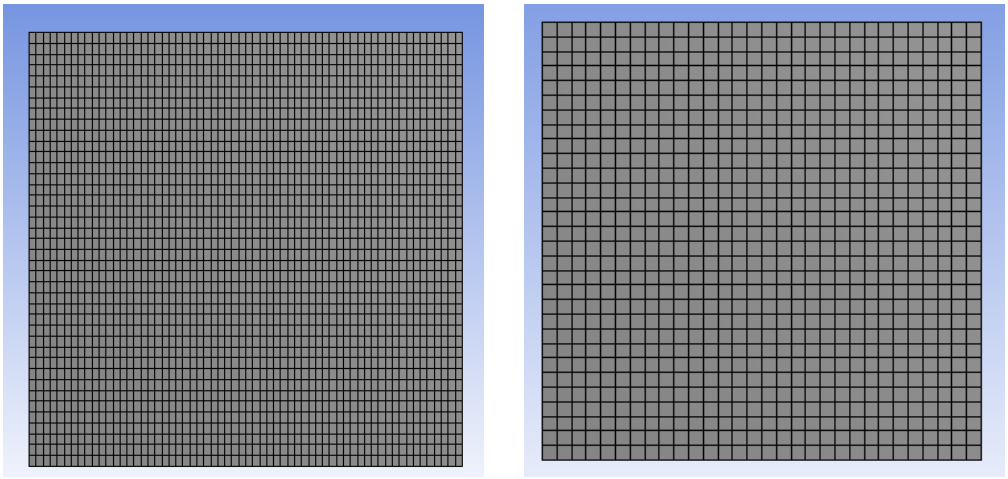

Figure 3-3 Mesh 30x30 and mesh 62x40

Table 3-1 Simulation parameters in ANSYS Fluent, Lid driven Cavity Flow

Option settings	**Selection**
Time	Transient
Models	Viscous - Laminar
Material	User defined
Density	1 kg/m3
Viscosity	Re=3,200 μ=0.0003125 Re=10,000 μ=0.0001
Moving lid wall	Absolute speed 1 m/s
Shear condition	No slip
Residuals Criteria	0.001
Time step size	0.1
Number of time steps	1500
Max iterations	30
Autosave every	300

In addition, 3-D simulation has been done to compare with the 2-D results. Figure 3-4 shows the geometry of the cavity. Figure 3-5 shows the mesh, and the simulation parameters are similar to the 2-D setup.

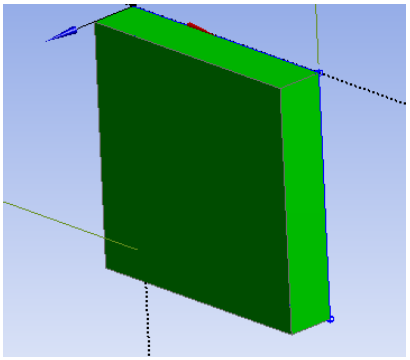

Figure 3-4 3-D geometry of the cavity, 1m x 1m x 0.2m

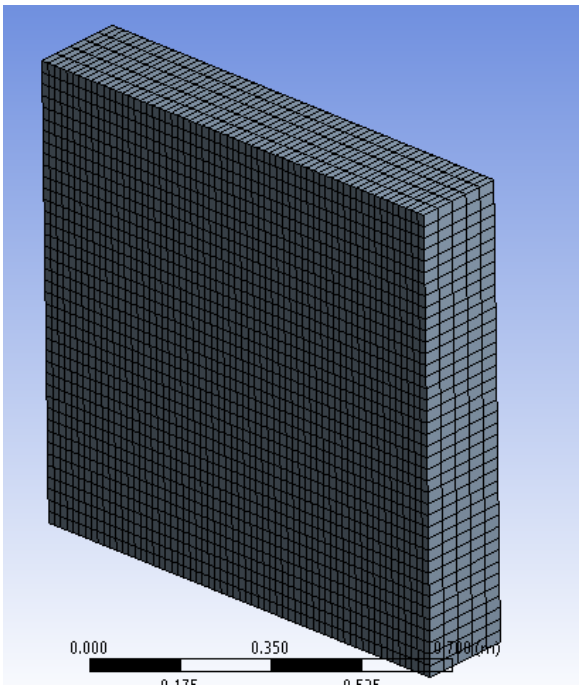

Figure 3-5 Mesh 62m x 40m x 5m

3.5.2 Flow Around A Circular Cylinder

First the “Geometry” module in ANSYS Fluent has been used to create the 2-D geometry of the cylinder. In order to construct a geometry similar to Allievi and Bermejo [2], for the first case, the cylinder diameter (D) has been set equal to 1m, the length of the control volume to 19.65m and the height to 9m. Figure 3-6 shows the 2-D cylinder geometry for the first case. Besides this geometry, in an attempt to attain more accurate results, a second case has been defined with larger geometry. For this case, the length of the control volume has been set to 40m and the height to 18m and the rest of the dimensions are similar to the first case. Figure 3-7 shows the 2-D cylinder geometry for the second case. Finally, a 3-D geometry has been created with dimensions similar to the first case of the 2-D geometry, and a depth of 1m. Figure 3-8 shows the 3-D cylinder geometry.

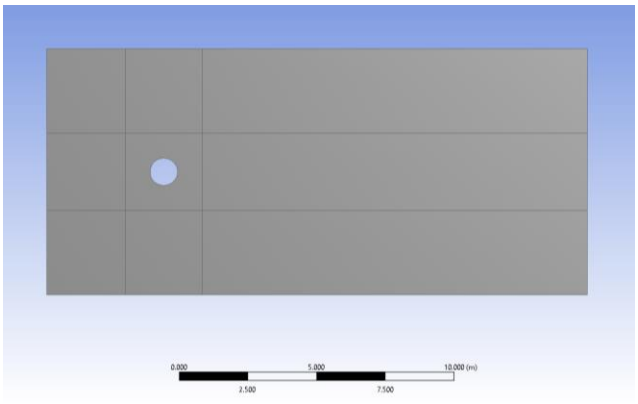

Figure 3-6 The 2-D cylinder geometry, first case, 19.65D x 9D

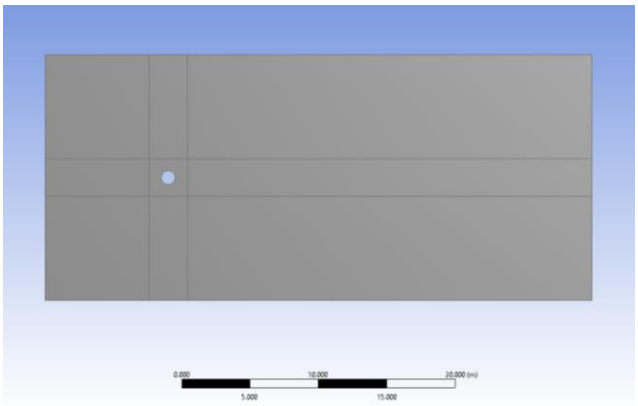

Figure 3-7 The 2-D cylinder geometry, second case, 40D x 18D

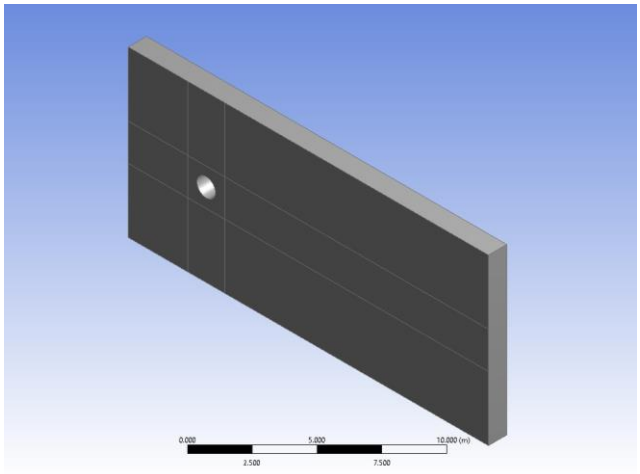

Figure 3-8 The 3-D cylinder geometry, 19.65D x 9D x 1D

Next, using the “Mesh” module, for the first case a mesh with 1340 elements have been defined to match those of Allievi and Bermejo [2] as close as possible. Figure 3-9 shows the 50x24 mesh for this

case. The same number of elements have been used for the second 2-D case. When compared to the first case, the mesh density in the areas close to the cylinder has been preserved, but since the same number of elements have been used for a larger geometry, the mesh in other areas has become more coarse. Figure 3-10 shows the areas where the mesh density is similar between the first and second cases and Figure 3-11 shows the 50x24 mesh for the second case. Figure 3-12 shows the 50x24x5 mesh for the 3-D cylinder.

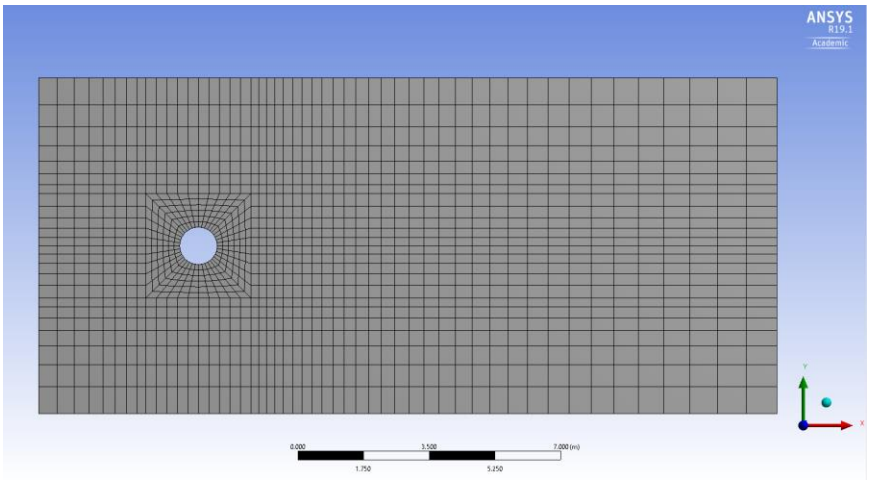

Figure 3-9 The 2-D cylinder geometry, first case, 50 x 24 mesh

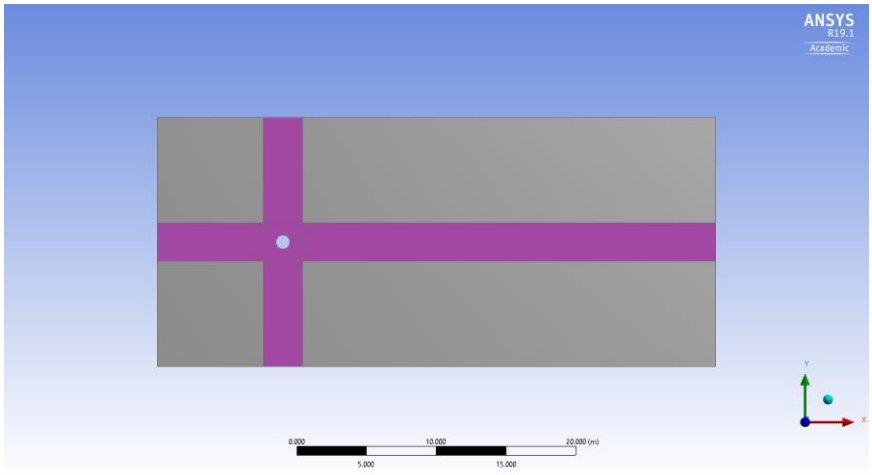

Figure 3-10 The 2-D cylinder geometry, similar mesh area

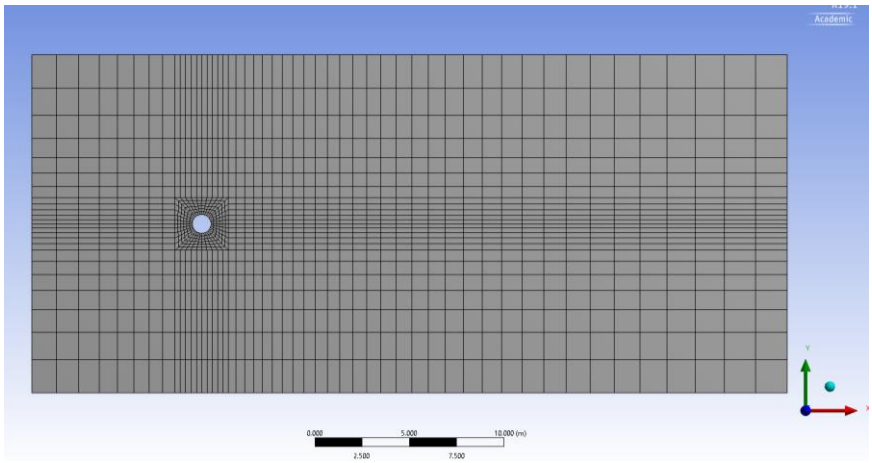

Figure 3-11 The 2-D cylinder geometry, second case, 50 x 24 mesh

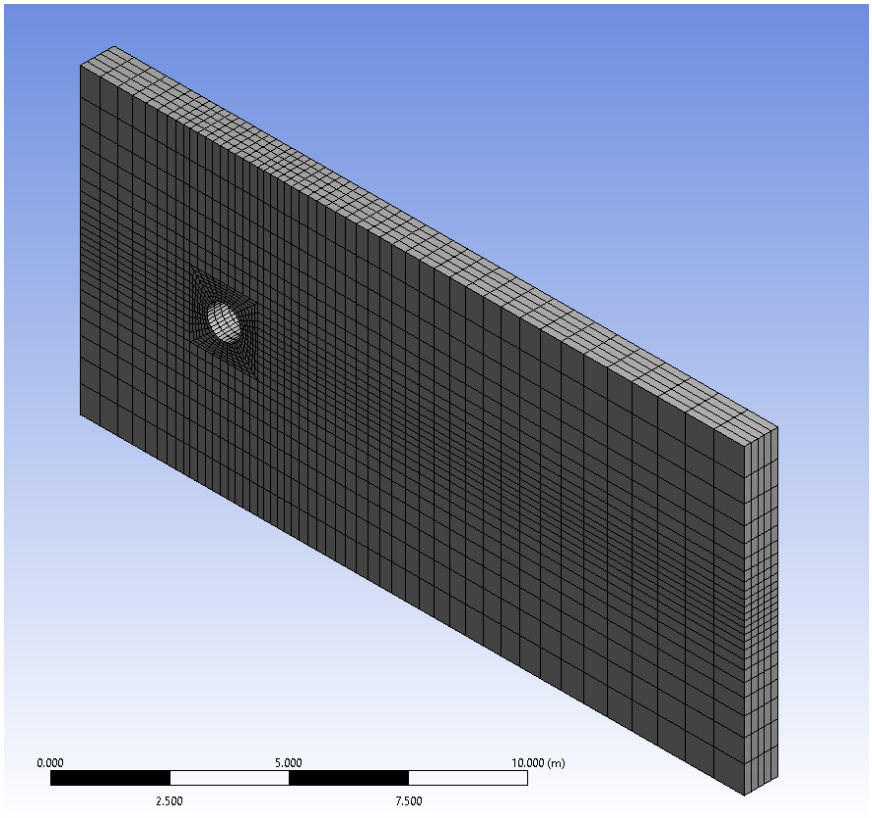

Figure 3-12 The 3-D cylinder geometry, 50 x 24 x 5 mesh

The simulation parameters have been set in the “Setup” module, and shown in Table 3-2. These values which are similar for both 2-D and 3-D cases, have been chosen in such a way as to match the Reynold number, Residual criteria and other problem characteristics used in Allievi and Bermejo [2]. Finally the simulation has been run until convergence was achieved.

Table 3-2 Simulation parameters in ANSYS Fluent, Flow over Circular Cylinder

Option settings	**Selection**
Time	Transient
Models	Viscous - Laminar
Material	User defined
Density	1 kg/m3
Viscosity	Re=100 μ=0.01
Inlet Velocity	Absolute speed in x: 1 m/s
Shear condition	No slip
Residuals Criteria	0.001
Time step size	0.1
Number of time steps	3000
Max iterations	30
Autosave every	100

CHAPTER 4: DISCUSSION OF RESULTS

4.1 Lid-Driven Square Cavity Flow

After each simulation run, for a different Reynolds Number, the average number of iterations were calculated between t= 0 s and a particular time step at which the code starts to converge with only a

single iteration. From Table 4-1, it can be observed that the average number of Iterations decreases in the beginning, then it slightly increases at around Re= 6000, and next it becomes nearly stable with further increase in the Reynolds number. Although the average number of Iterations differ when compared with Allievi and Bermejo [2], due to the distinct simulation codes used, but it shows a similar pattern.

Table 4-1 Average Number of Iterations, Lid-Driven Cavity Flow

Re= 100	**Re= 1000**	**Re= 2000**	**Re= 3200**	**Re= 5000**	**Re= 6000**	**Re= 8000**	**Re= 10,000**
12.73	11.47	10.26	8.33	7.97	8.02	7.93	7.12

Further, streamlines were plotted for the 62×40 Mesh at Re= 3200 and Re= 10,000 and the results were compared to the respective results of Allievi and Bermejo [2]. At both Reynold's Numbers, the streamlines and vortices showed almost the same flow behaviour as with the published data.

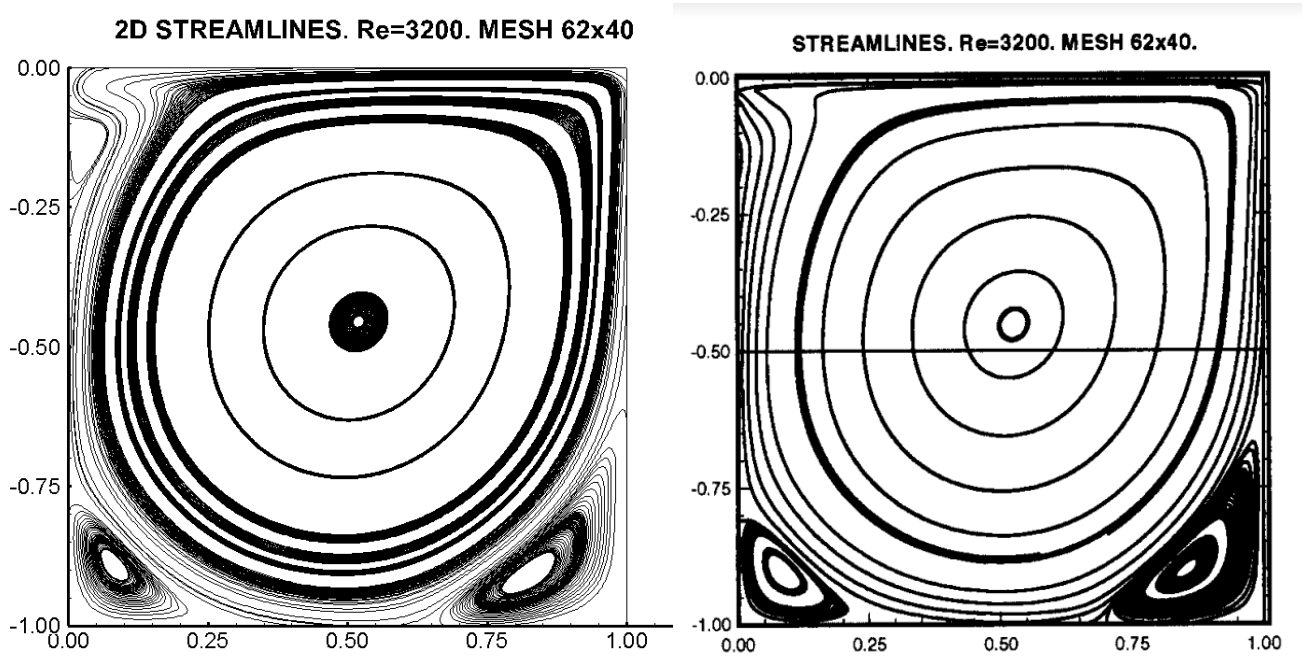

Figure 4-1 Cavity flow for 2-D at Re= 3200 compared with result of Ref.2 (Right)

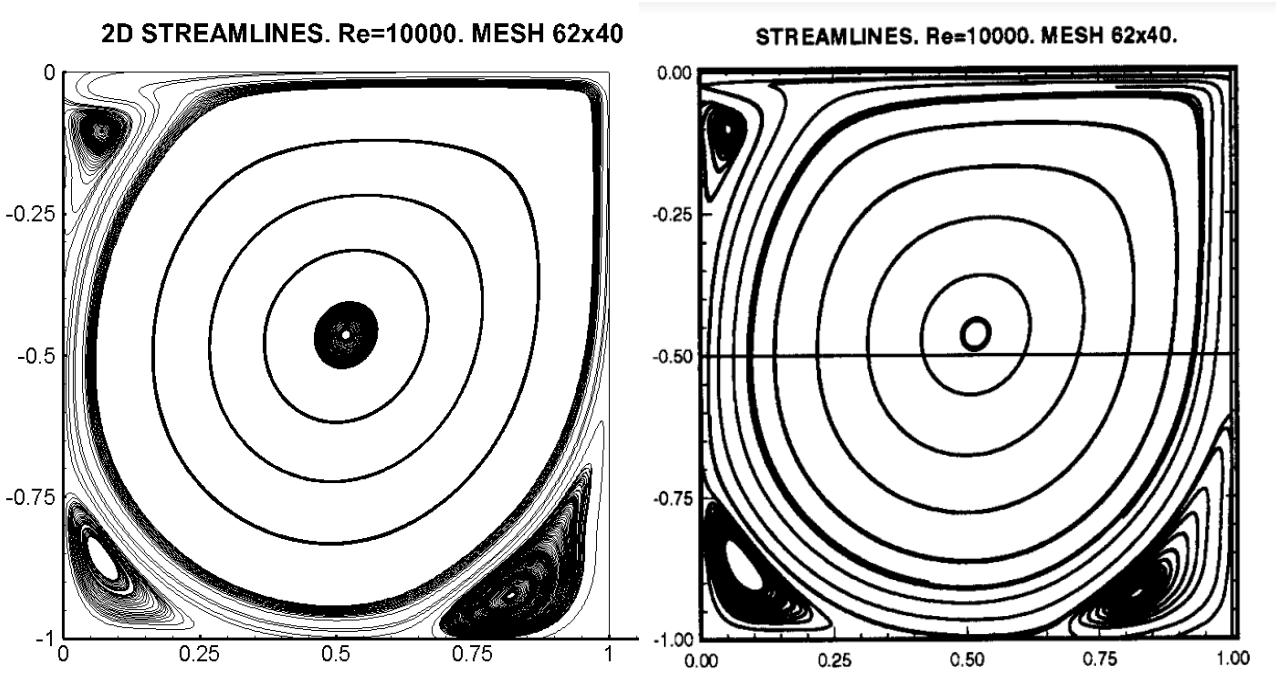

Figure 4-2 Cavity flow for 2-D at Re= 10000, compared with result of Ref.2 (Right)

To further examine the phenomenon, a 3-D case was considered for the 62×40×20 Mesh at Re= 3200 and Re= 10,000, where a significant whirling effect of fluid was observed for the higher Re and there were no signs of any instabilities. Almost identical results were also presented by Koseff and Street [7].

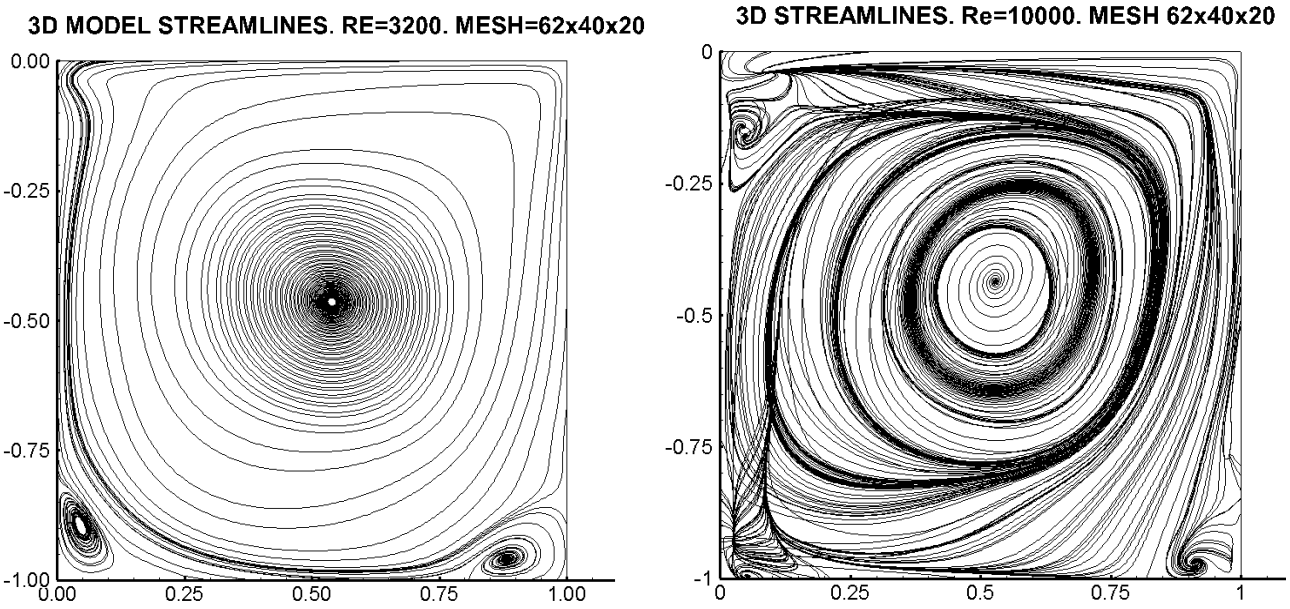

Figure 4-3 Cavity flow for 3-D at Re= 3200 and Re= 10,000

Moreover, the velocity profiles along the mid-horizontal and mid-vertical lines, at Re= 3200 and Re= 10,000, were computed. All the results have been plotted (Fig.4-4 to Fig. 4-9) for both the 2-D and 3-D cases and are in good agreement with Allievi and Bermejo [2] as well as Ghia .et. al.[22] for 2-D and with Koseff and Street for 3-D [6,7].

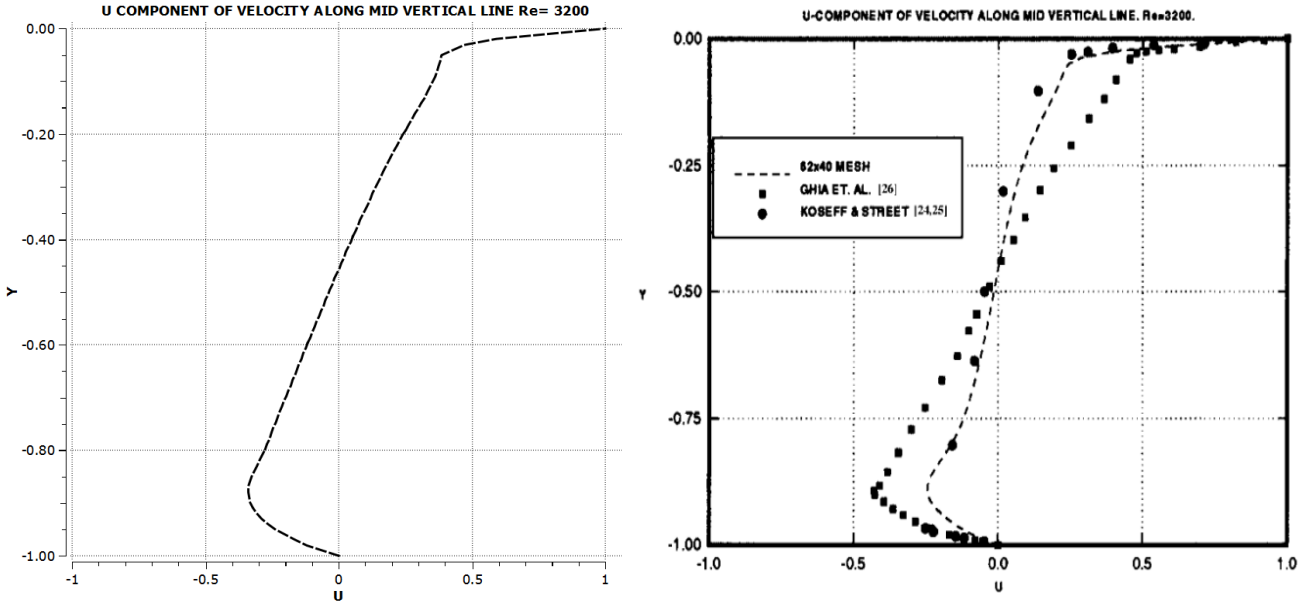

Figure 4-4 Cavity Flow for 2-D. Re= 3200. Velocity profiles at Mid Vertical Line compared with Ref 2.

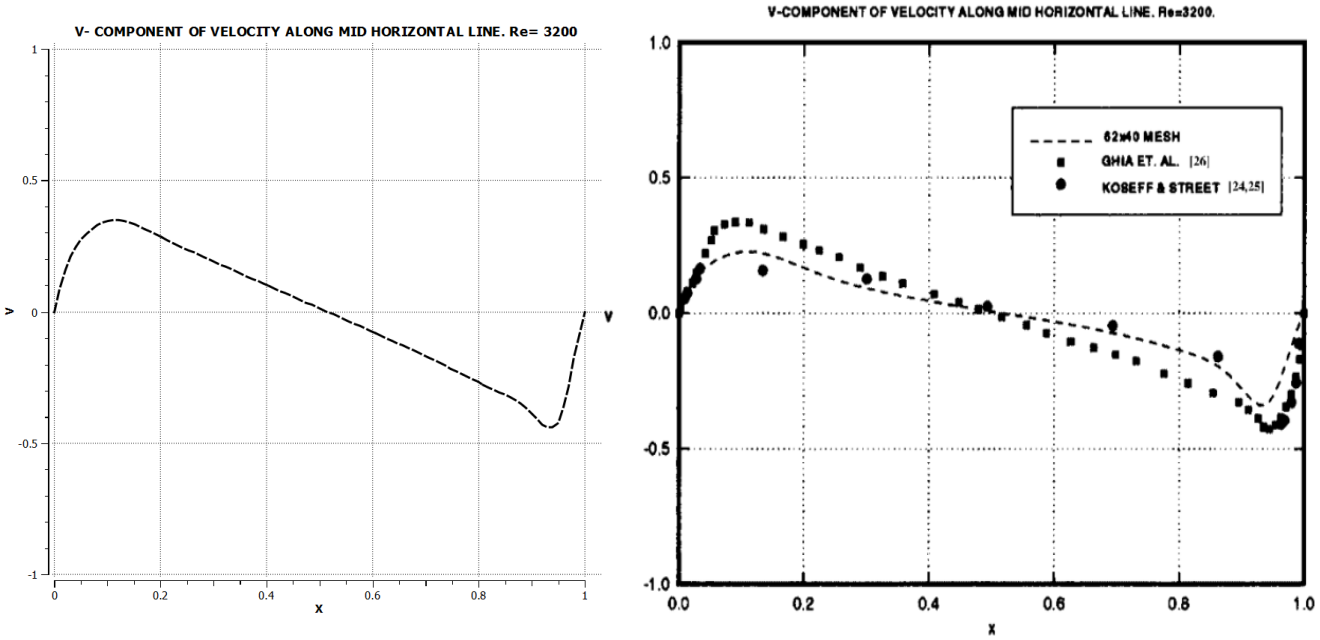

Figure 4-5 Cavity Flow for 2-D. Re= 3200. Velocity profiles at Mid Horizontal Line compared with Ref 2.

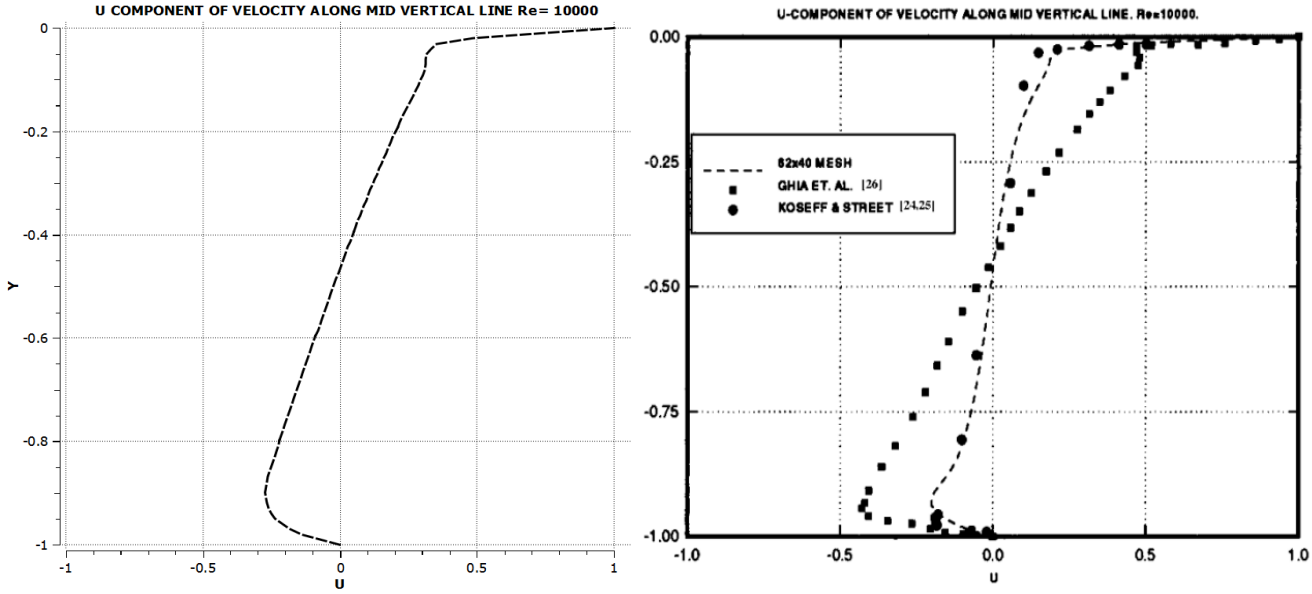

Figure 4-6 Cavity Flow for 2-D. Re= 10,000. Velocity profiles at Mid Vertical Line compared with Ref 2.

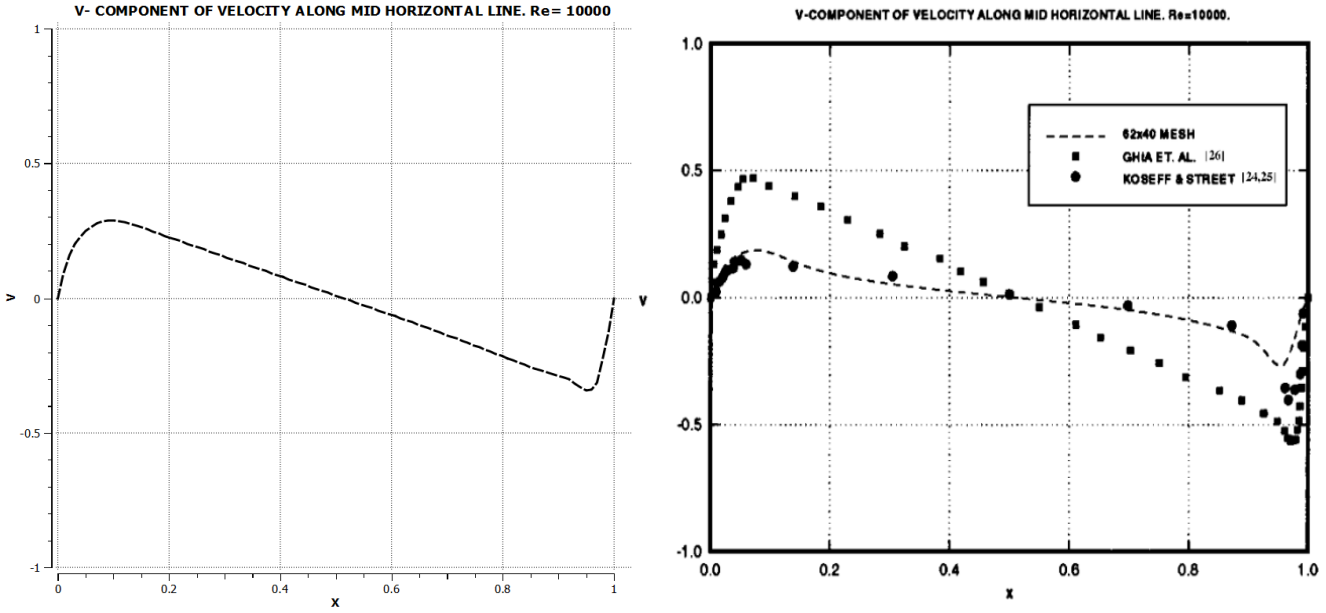

Figure 4-7 Cavity Flow 2-D. Re= 10,000. Velocity profiles at Mid Horizontal Line compared with Ref 2.

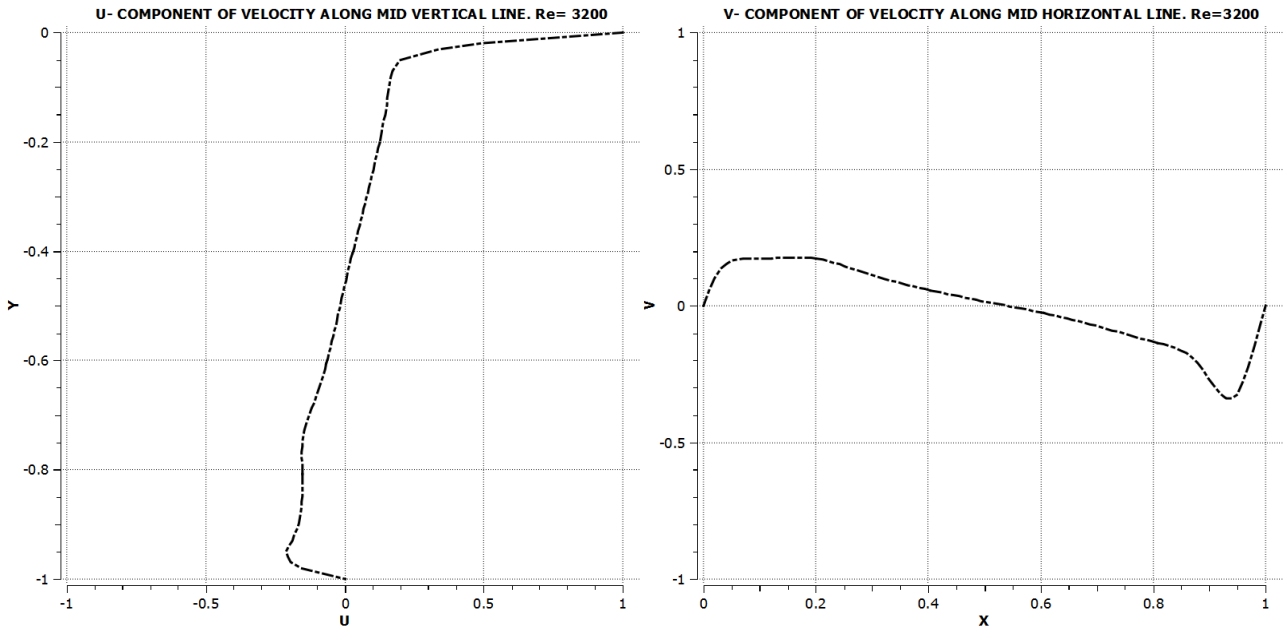

Figure 4-8 Cavity Flow for 3-D. Re= 3200. Velocity profiles at Mid Vertical and Horizontal Line

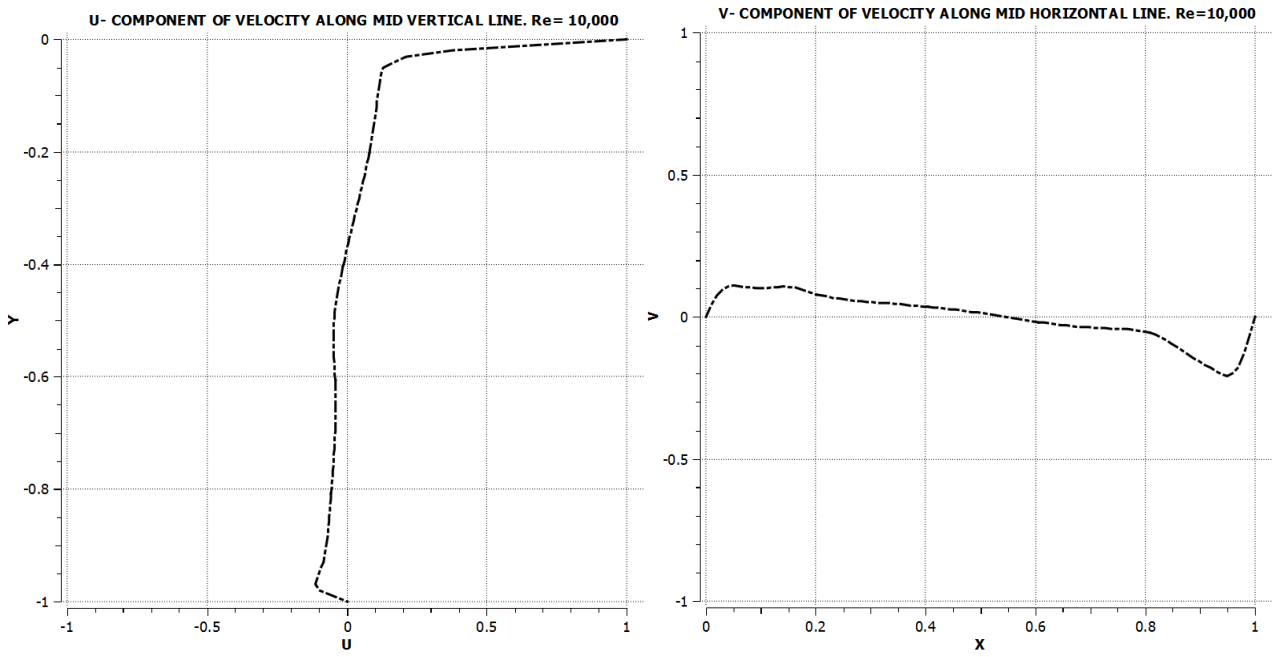

Figure 4-9 Cavity Flow for 3-D. Re= 10,000. Velocity profiles at Mid Vertical and Horizontal Line

4.2 Flow Around A Circular Cylinder

After running the Ansys Fluent solver for the first 2-D case and plotting the streamlines, excellent agreement was achieved with Allievi and Bermejo [2]. Figure 4-10 shows the streamlines of the flow at different time steps for this work (on the left side) and for Allievi and Bermejo [2] (on the right side).

Two symmetric vortices form behind the cylinder, and they start to grow with time until they become asymmetric around t=20 s. later they start becoming unstable and shed alternatively and create the well-known Karman street.

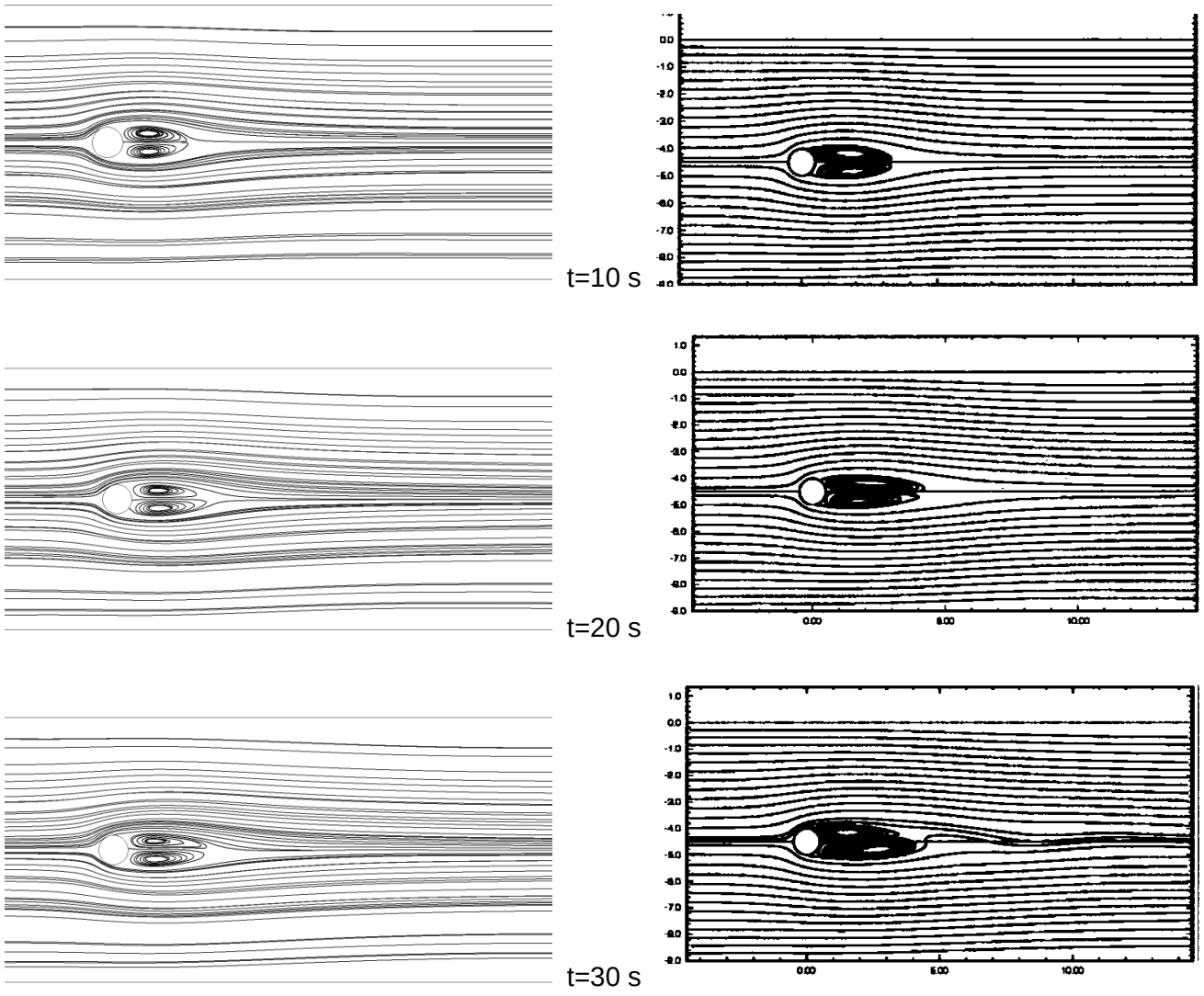

Figure 4-10 Streamlines for the 2-D cylinder, case 1 on the left, Ref.2 on the right

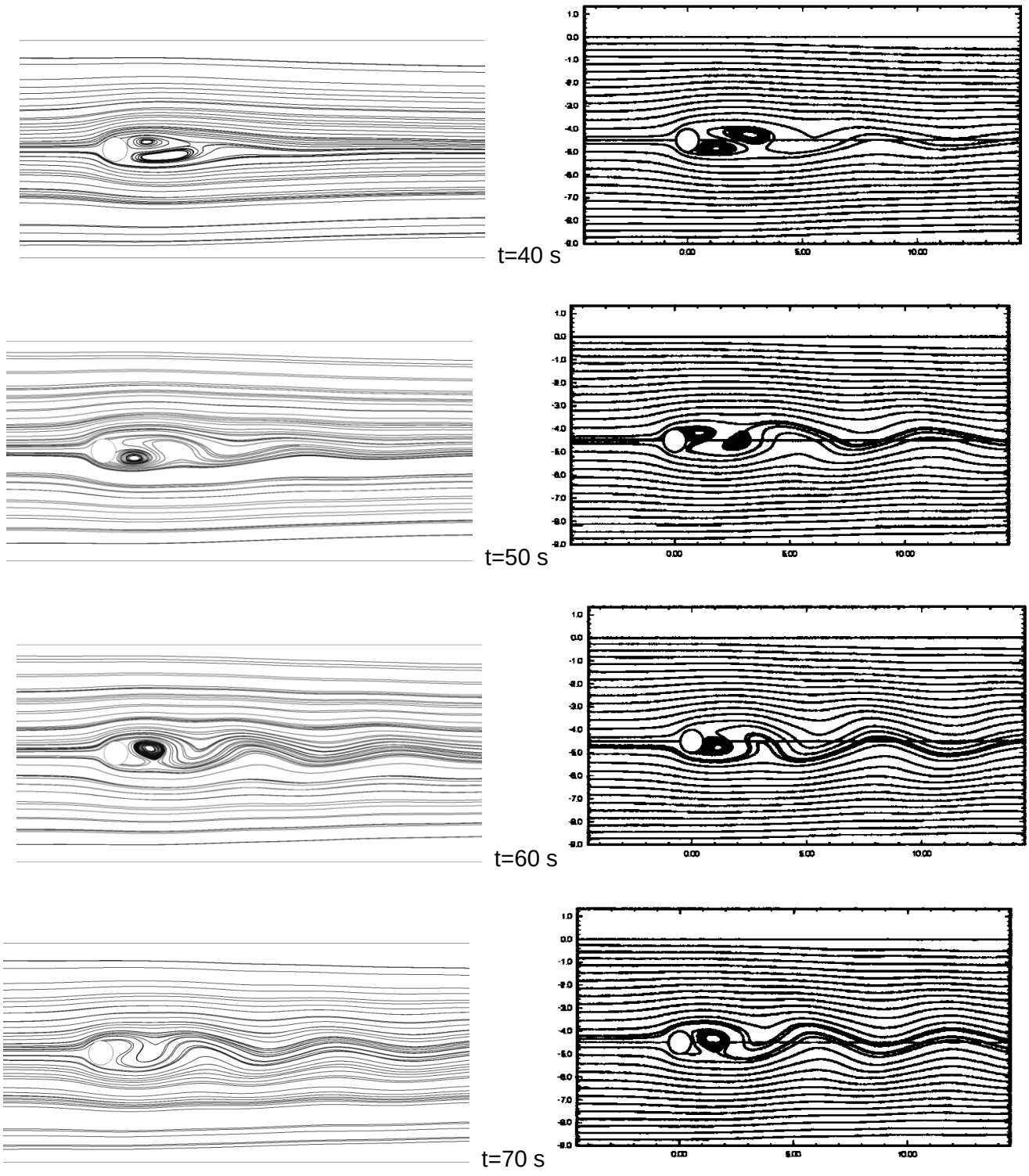

Figure 4-10 Streamlines for the 2-D cylinder, case 1 on the left, Ref.2 on the right (Continued)

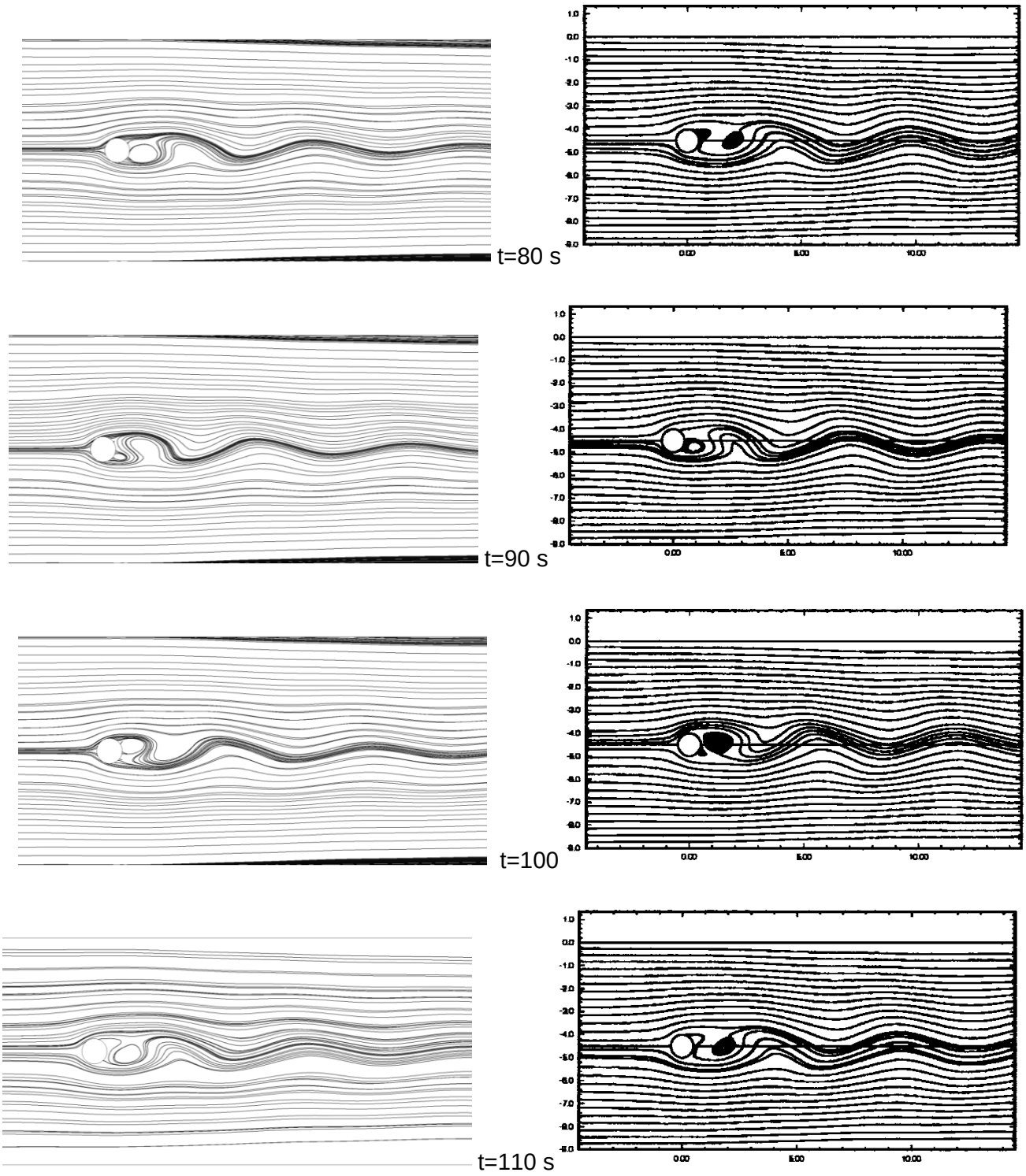

Figure 4-10 Streamlines for the 2-D cylinder, case 1 on the left, Ref.2 on the right (Continued)

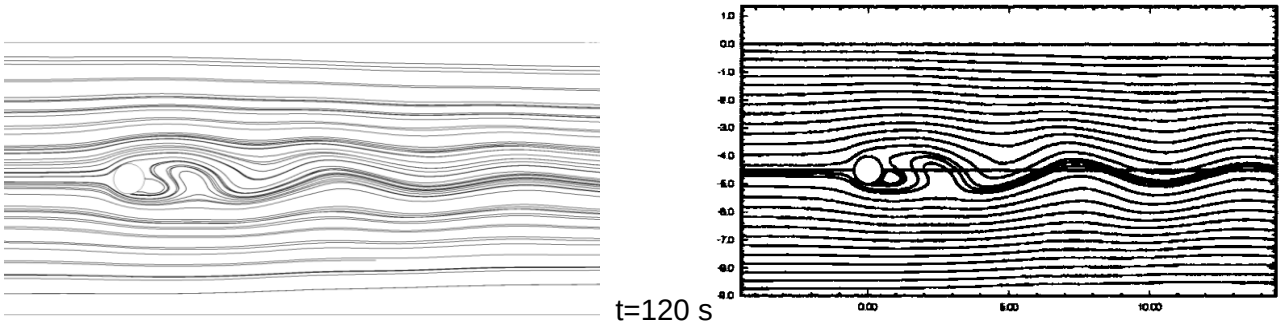

Figure 4-10 Streamlines for the 2-D cylinder, case 1 on the left, Ref.2 on the right (Continued)

The force coefficients were plotted and were close to the results of Allievi and Bermejo [2]. Figure 4-11 shows the force coefficients for the first case. Looking at this plot, lift coefficient is zero for the first 20 second, and then it starts to exhibit its oscillatory nature. these oscillations grow in amplitude and become stable after around 80 seconds. The Strouhal number of the oscillations in this region is 0.17. Furthermore it can be mentioned that the drag coefficient has also an oscillatory nature, and the frequency is higher than that of the lift coefficient. The mean drag coefficient is calculated to be 1.492 from which 1.192 (or about 80%) is due to pressure, and 0.3 (or about 20%) based on viscous forces. Figure 4-12 displays the force coefficients for Allievi and Bermejo [2] for comparison.

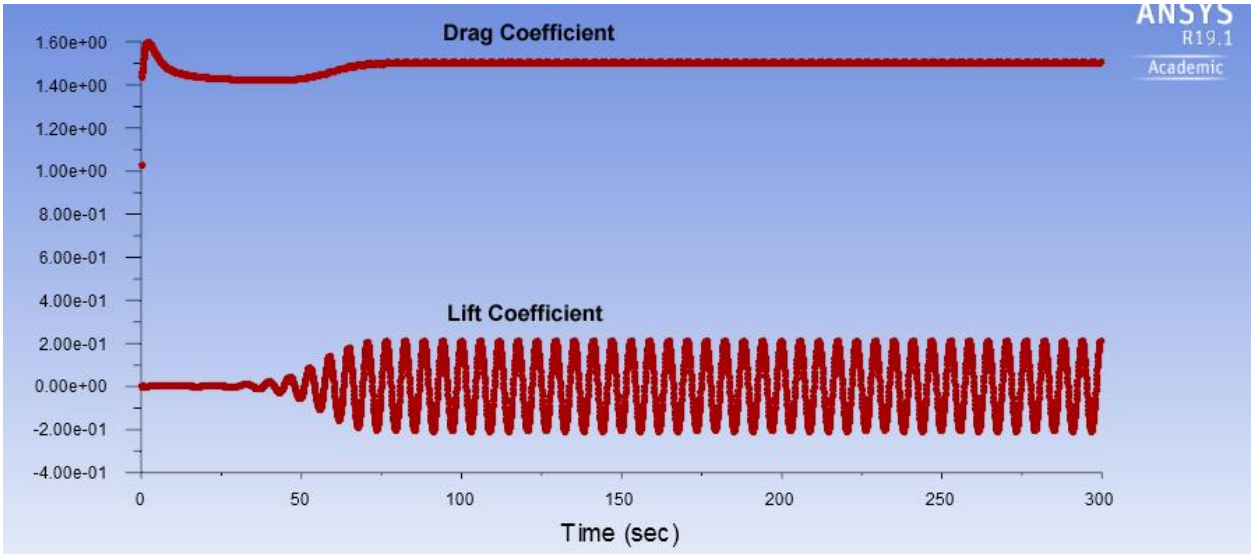

Figure 4-11 Force Coefficients for the 2-D cylinder, case 1, Re=100

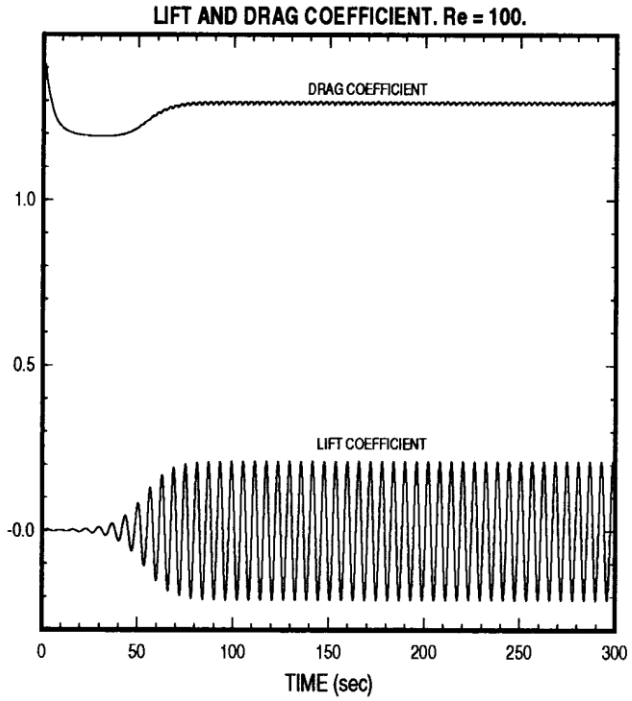

Figure 4-12 Force Coefficients for the 2-D cylinder, Ref.2, Re=100

Although the results of the previous case were close to those of Allievi and Bermejo [2], but we tried to achieve even better results by running Ansys Fluent solver for multiple different finer meshes and shorter timesteps. The best result was obtained by using a larger control volume to capture the flow characteristics further away from the cylinder body without changing the number of mesh elements as explained in 3.5.2. By running the simulation for this second 2-D case and plotting the streamlines, excellent agreement was achieved with the Ref 2 and the mean value of the drag coefficient became noticeably more accurate. Figure 4-13 shows the streamlines of the flow at different time steps which are similar in nature to the first case.

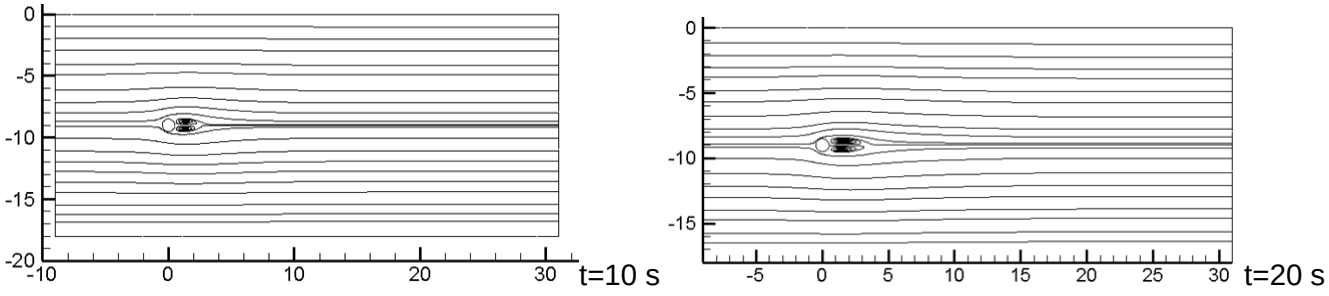

Figure 4-13 Streamlines for the 2-D cylinder, case 2, Re=100

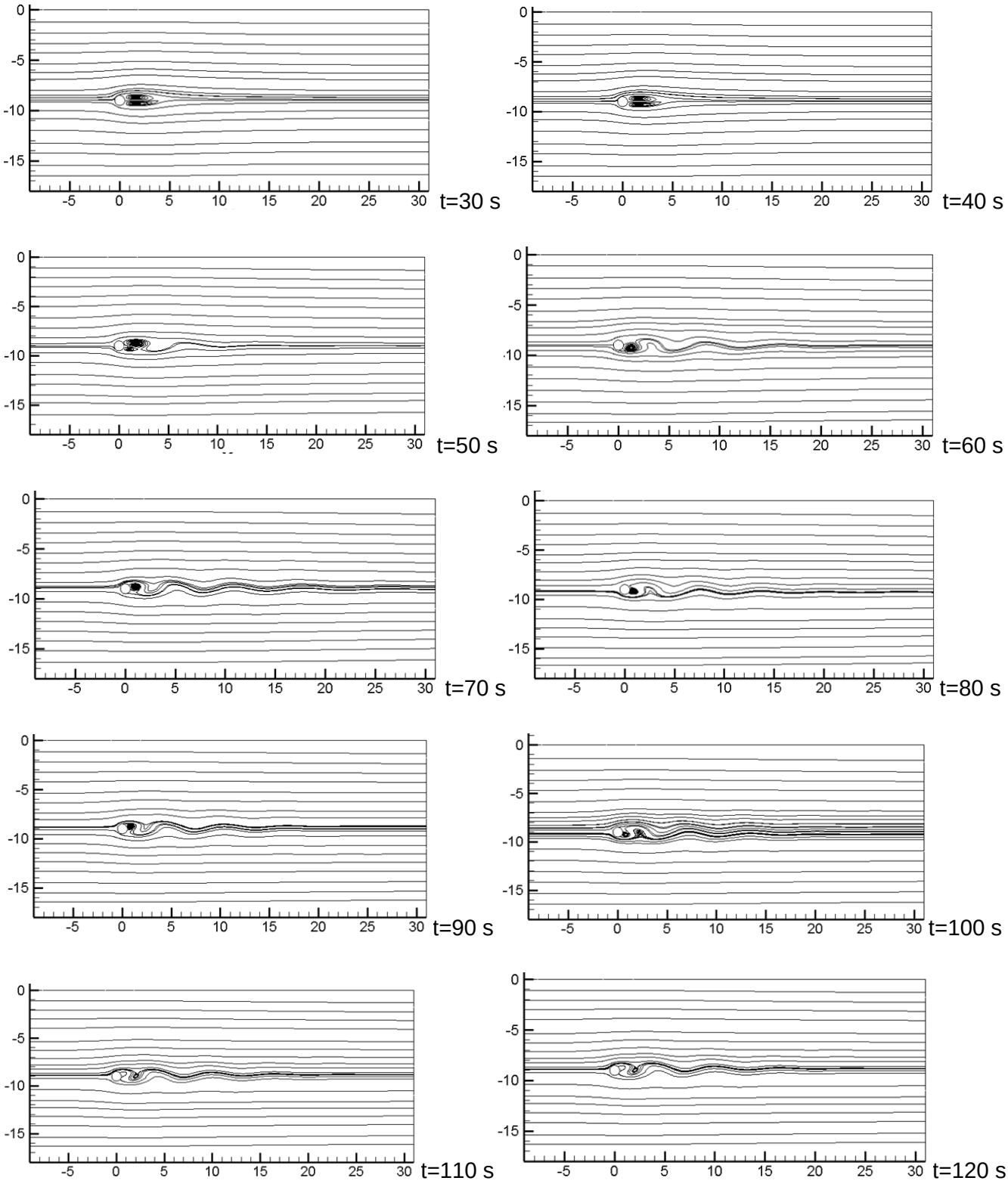

Figure 4-13 Streamlines for the 2-D cylinder, case 2, Re=100 (Continued)

Figure 4-14 shows the force coefficients for the second case which are similar in nature to the first case. The mean drag coefficient is calculated to be 1.310 from which 1.035 (or about 80%) is due to pressure, and 0.275 (or about 20%) based on viscous forces.

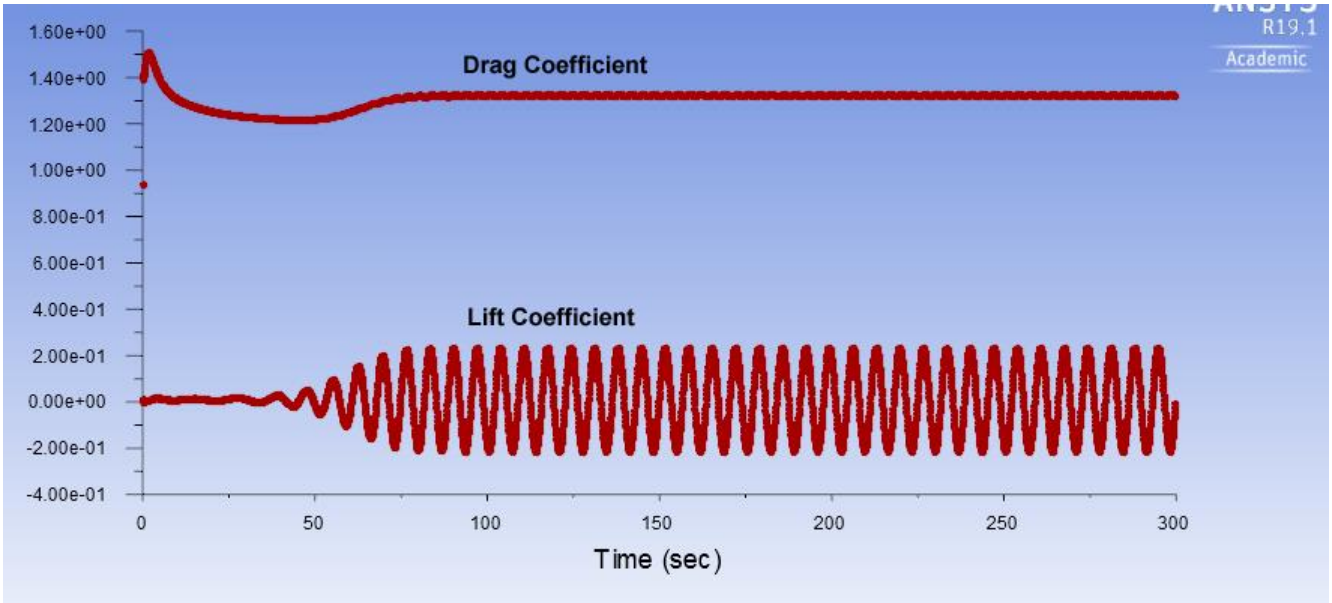

Figure 4-14 Force Coefficients for the 2-D cylinder, case 2, Re=100

Finally, running the simulation for the 3-D cylinder and plotting the streamlines, again excellent agreement was achieved with Allievi and Bermejo [2]. Figure 4-15 shows the streamlines of the flow at different time steps which are similar in nature to the 2-D cases.

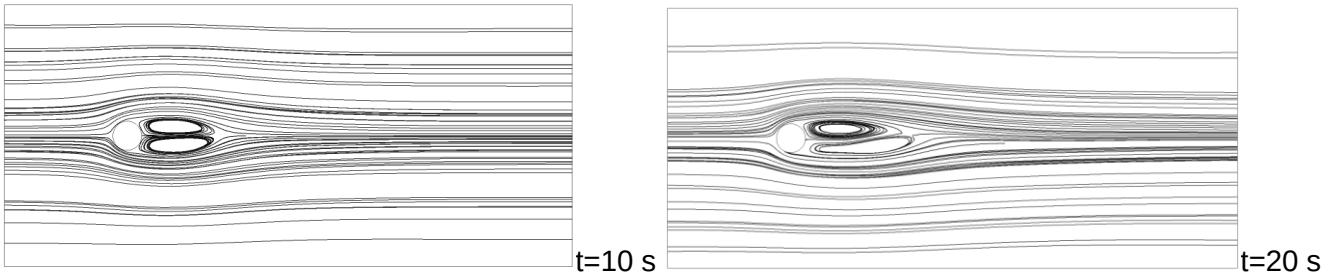

Figure 4-15 Streamlines for the 3-D cylinder, Re=100

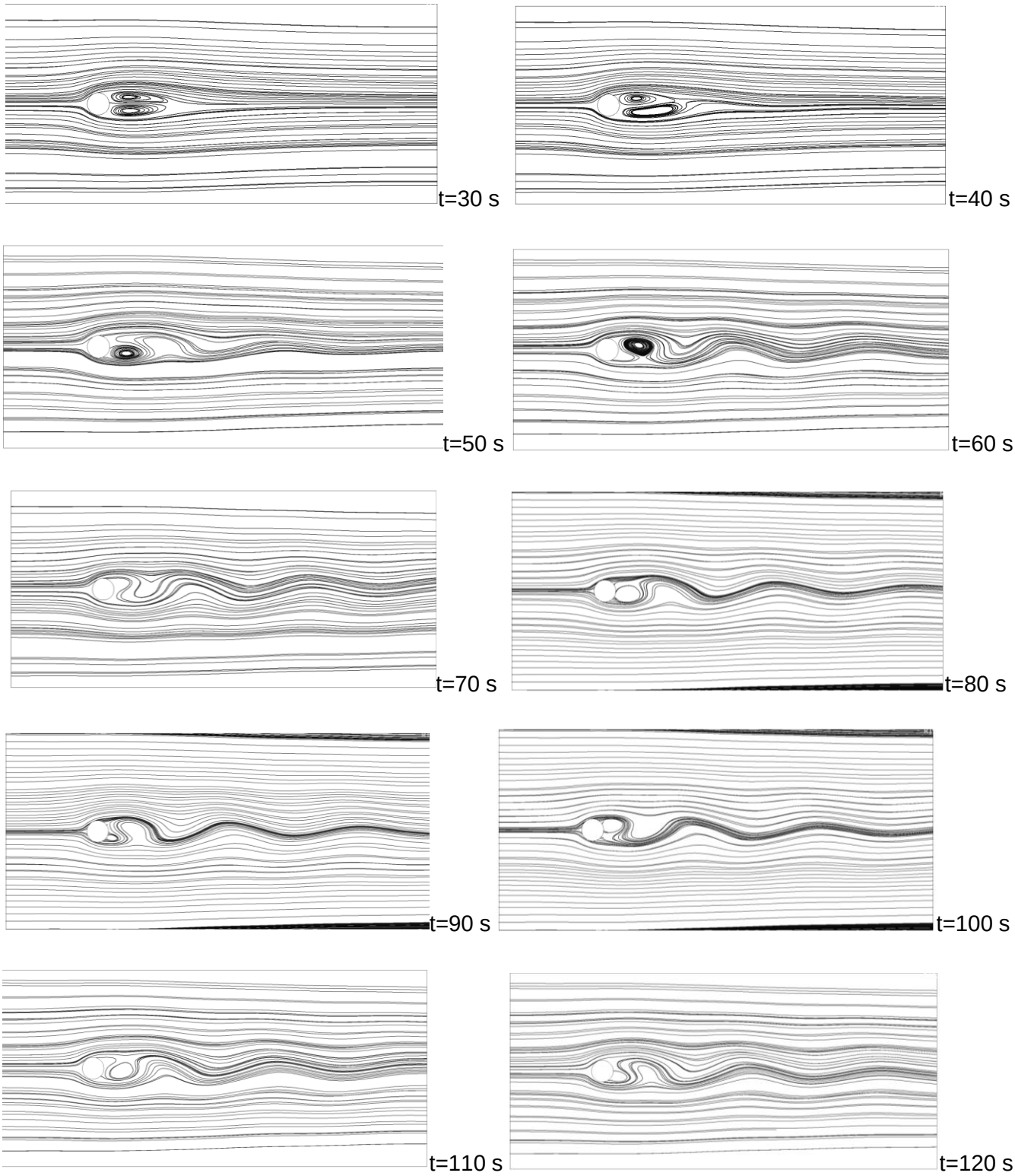

Figure 4-15 Streamlines for the 3-D cylinder, Re=100 (Continued)

The force coefficients were plotted in Figure 4-16 and although the mean dag coefficient was larger, but it was still within a reasonable approximation from the 2-D cases and Allievi and Bermejo [2]. We

certainly did not expect to achieve the exact same results for the 3-D case, but the fact that these results are in the same ballpark as the 2-D cases, shows that the 3-D simulation has been correctly implemented. In order to further improve the results for the 3-D simulation in the future, running the simulation on finer meshes as well as larger control volumes can be tested. Figure 4-16 shows the force coefficients for the 3-D cylinder which are similar in nature to the 2-D cases. The mean drag coefficient is calculated to be 1.586 from which 1.251 (or about 80%) is due to pressure, and 0.335 (or about 20%) based on viscous forces.

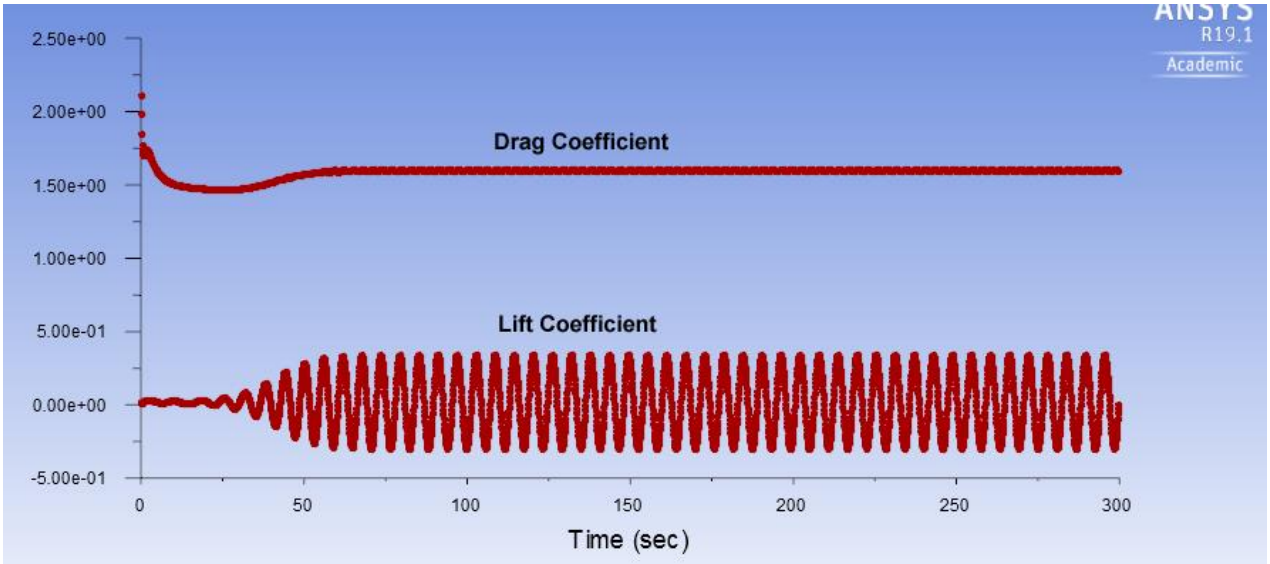

Figure 4-16 Force Coefficients for the 3-D cylinder, Re=100

In summary, Table 4-2 compares these results with experimental and numerical data presented by Graham [31] and Allievi and Bermejo [2]. Good agreement is observed for all the variables.

Table 4-2 Comparison of Results, Flow over Circular Cylinder

	Graham [31]	Allievi and Bermejo [2]	This work, 2-D First Case	This work, 2-D Second Case	This work, 3-D
Strouhal number	0.160	0.167	0.170	0.176	0.245
Mean drag coefficient	1.25 - 1.46	1.295	1.492	1.310	1.586
RMS of fluctuating drag coefficient	0.0042 - 0.04	0.0085	0.040	0.040	0.042
RMS of fluctuating lift coefficient	0.157 - 0.39	0.162	0.140	0.140	0.209

CHAPTER 5: CONCLUSION

Ansys Fluent has been used to simulate two different unsteady incompressible viscous flow cases; A lid driven cavity flow and the flow around a circular cylinder. The geometry and mesh characteristics of both cases have been chosen in such a way as to closely mimic that of Allievi and Bermejo [2] and all variables presented in the results for the two cases were in good agreement with published data. Next, for the case of the circular cylinder, different mesh and geometries were tried out and more accurate results were obtained using a larger control volume while preserving the number of mesh elements. Finally, three-dimensional simulations have been run for both cases and good agreement was obtained with the two-dimensional cases, as well as the published data.

REFERENCES

[1] Zuo, W. (2005). Introduction of Computational Fluid Dynamics. St. Petersburg.

[2] Allievi, A., & Bermejo, R. (2000). Finite Element Modified Method of Characteristics for the Navier–Stokes Equations. Int. J. Numer. Methods Fluids 32, 439–464.

[3] Nakayama, Y. (2018). Introduction to Fluid Mechanics (2nd ed.). Oxford, British: Butterworth-Heinemann,

[4] Moukalled, F., Mangani, L., & Darwish, M. (2016). The Finite Volume Method in Computational Fluid Dynamics. An Advanced Introduction with OpenFOAM and Matlab, 3-8.

[5] Akyuzlu, K. M. (2017, November). A Numerical and Experimental Study of Laminar Unsteady Lid-Driven Cavity Flows. Paper presented at the ASME 2017 International Mechanical Engineering Congress and Exposition, Tampa, Florida, USA (pp. V007T09A015-V007T09A015).

[6] Koseff, J. R., & Street, R. L. (1984). The Lid-Driven Cavity Flow: A Synthesis of Qualitative and Quantitative Observations. Journal of Fluids Engineering, 106(4), 390-398.

[7] Koseff, J. R., & Street, R. L. (1984). On End Wall Effects in A Lid-Driven Cavity Flow. Journal of fluids engineering, 106(4), 385-389.

[8] Migeon, C. (2002). Details on the Start-Up Development of the Taylor-Gortler-Like Vortices Inside A Square-Section Lid-Driven Cavity for 1,000≤ Re ≤ 3,200. Experiments in Fluids, 33(4), 594-602.

[9] Causon, D.M., & Mingham, C. G. (2010). Introductory Finite Difference Methods for PDEs (1st ed.). Bookboon.

[10] Bruneau, C. H., & Saad, M. (2006). The 2D Lid-Driven Cavity Problem Revisited. Computers & Fluids, 35(3), 326-348.

[11] Moukalled, F., Mangani, L., & Darwish, M. (2016). The Finite Volume Method in Computational Fluid Dynamics. An Advanced Introduction with OpenFOAM and Matlab, 3-8.

[12] Wright, N. G., & Gaskell, P. H. (1995). An Efficient Multigrid Approach to Solving Highly Recirculating Flows. Computers & Fluids, 24(1), 63-79.

[13] Vanka, S. P. (1986). Block-Implicit Multigrid Solution of Navier-Stokes Equations in Primitive Variables. Journal of Computational Physics, 65(1), 138-158.

[14] Liu, G. R., & Quek, S. S. (2013). The Finite Element Method: A Practical Course. Butterworth-Heinemann.

[15] Barragy, E., & Carey, G. F. (1997). Stream function-vorticity driven cavity solution using p finite elements. Computers & Fluids, 26(5), 453-468.

[16] Bozeman, J.D., & Dalton, C. (1973). Numerical Study of Viscous Flows in a Cavity. Journal of Computational Physics, 12, 348-363.

[17] Goodrich, J.W., & Soh, W.Y. (1989). Time-Dependent Viscous Incompressible Navier Stokes Equations: The Finite Difference Galerkin Formulation and Stream function Algorithms, Journal of Computational Physics, 84, 207-241.

[18] Iwatsu, R., Hyun, J. M., & Kuwahara, K. (1993). Numerical Simulations of Three Dimensional Flows in a Cubic Cavity with an Oscillating Lid, Journal of Fluids Engineering, 115, 680-686.

[19] Aguirre, A., Castillo, E., Cruchaga, M., Codina, R., & Baiges, J. (2018). Stationary and Time-Dependent Numerical Approximation of the Lid-Driven Cavity Problem for Power-Law Fluid Flows at High Reynolds Numbers using a Stabilized Finite Element Formulation of the VMS Type, J of Non-Newtonian Fluid Mech, 257, 22–43

[20] Jiang, C., Zhang, Z.Q., Han ,X., Liu, G., & Lin, T. (2018). A Cell-Based Smoothed Finite Element Method with Semi-Implicit CBS Procedures for Incompressible Laminar Viscous Flows, Int J Numer Meth Fluids, 86, 20–45

[21] Wang, Y., Shu, C., Yang, L., & Yuan H. (2016). A Decoupling Multiple-Relaxation-Time Lattice Boltzmann Flux Solver for Non-Newtonian Power-Law Fluid Flows, J. Non-Newtonian Fluid Mech, 235, 20–28

[22] Ghia, U., Ghia, K.N. & Shin , C.T. (1982). High-Re Solutions for Incompressible Flow using the Navier–Stokes Equations and a Multigrid Method, J. Comput. Phys., 48, 387–411

[23] Wahba, E. (2012). Steady Flow Simulations Inside a Driven Cavity up to Reynolds Number 35,000, Comput. Fluids, 66, 85–97

[24] Yapici, K., Uludag, Y. (2013). Finite Volume Simulation of 2-D Steady Square Lid Driven Cavity Flow at High Reynolds Numbers, Braz. J. Chem. Eng, 30, 923–937.

[25] Hua, Z., & Zheng, X. (2015). Fluid Flow in a Cavity Driven by an Oscillating Lid by an Improved Incompressible SPH, Procedia Engineering, 126, 275 – 279

[26] Soh, W.H., & Goodrich, J.W. (1988) Unsteady Solution of Incompressible Navier-Stokes Equations, J. Comput. Phys., 79, 113-134

[27] Harichandan, A. B., & Roy, A. (2010). Numerical Investigation of Low Reynolds Number Flow Past Two and Three Circular Cylinders Using Unstructured Grid CFR Scheme. International Journal of heat and fluid flow, 31(2), 154-171.

[28] Rajani, B. N., Kandasamy, A., & Majumdar, S. (2009). Numerical Simulation of Laminar Flow Past A Circular Cylinder. Applied Mathematical Modelling, 33(3), 1228-1247.

[29] Qu, L., Norberg, C., Davidson, L., Peng, S. H., & Wang, F. (2013). Quantitative Numerical Analysis of Flow Past A Circular Cylinder at Reynolds Number Between 50 and 200. Journal of Fluids and Structures, 39, 347-370.
[30] Source: SlidePlayer. Published byAshley Baker. https://slideplayer.com/slide/6663703/
[31] Arkell, R. H., & Graham, J. M. R. (1993). The Effects of Waves on Vortex Shedding from Cylinders. In Bluff-Body Wakes, Dynamics and Instabilities (pp. 19-22). Springer, Berlin, Heidelberg.